AD NUMBER
AD907690
LIMITATION CHANGES
TO: **Approved for public release; distribution is unlimited.**
FROM: **Distribution authorized to U.S. Gov't. agencies only; Test and Evaluation; JAN 1973. Other requests shall be referred to Air Force Armament Laboratory DLIV, Eglin AFB, FL 32542.**
AUTHORITY
afal ltr, 24 jun 1974

AEDC-TR-73-20

11.8

HEAT-TRANSFER TESTS USING THERMOGRAPHIC PHOSPHOR PAINT ON THE HIGH ALTITUDE SUPERSONIC TARGET (HAST) MISSILE AT MACH NUMBER 4

E. C. Knox and L. D. Carter

ARO, Inc.

February 1973

VON KÁRMÁN GAS DYNAMICS FACILITY
ARNOLD ENGINEERING DEVELOPMENT CENTER
AIR FORCE SYSTEMS COMMAND
ARNOLD AIR FORCE STATION, TENNESSEE

NOTICES

When U. S. Government drawings specifications, or other data are used for any purpose other than a definitely related Government procurement operation, the Government thereby incurs no responsibility nor any obligation whatsoever, and the fact that the Government may have formulated, furnished, or in any way supplied the said drawings, specifications, or other data, is not to be regarded by implication or otherwise, or in any manner licensing the holder or any other person or corporation, or conveying any rights or permission to manufacture, use, or sell any patented invention that may in any way be related thereto.

Qualified users may obtain copies of this report from the Defense Documentation Center.

References to named commercial products in this report are not to be considered in any sense as an endorsement of the product by the United States Air Force or the Government.

HEAT-TRANSFER TESTS USING THERMOGRAPHIC PHOSPHOR PAINT ON THE HIGH ALTITUDE SUPERSONIC TARGET (HAST) MISSILE AT MACH NUMBER 4

E. C. Knox and L. D. Carter
ARO, Inc.

FOREWORD

The work reported herein was conducted at the Arnold Engineering Development Center (AEDC) under sponsorship of the Air Force Flight Dynamics Laboratory (AFFDL), Air Force Systems Command (AFSC), for the Air Force Armament Laboratory (AFATL), Eglin Air Force Base, Florida, under Program Element 63232F, System 469A.

The results presented herein were obtained by ARO, Inc. (a subsidiary of Sverdrup & Parcel and Associates, Inc.), contract operator of AEDC, AFSC, Arnold Air Force Station, Tennessee. The tests were conducted on February 21 and 22, 1972, under ARO Project No. VA014. The manuscript was submitted for publication on August 28, 1972.

The authors wish to express their gratitude to Mr. T. D. Buchanan for his assistance during the testing phase of this program, Mr. W. C. Armstrong for the theoretical pressure distributions used in the heat-transfer theoretical calculations, and Dr. A. W. Mayne, Jr., for providing those calculations.

This technical report has been reviewed and is approved.

JIMMY W. MULLINS
Lt Colonel, USAF
Chief Air Force Test Director, VKF
Directorate of Test

A. L. COAPMAN
Colonel, USAF
Director of Test

ABSTRACT

Thermographic phosphor heat-transfer tests were made on two models (0.5-scale and 0.25-scale) of the High Altitude Supersonic Target (HAST) missile at Mach number 4 and a Reynolds number, based on model length, of 21×10^6. Angle of attack was varied from 0 to 12 deg; effects of canard settings of 0 and 15 deg for the 0.25-scale model and 0, 5, 10, and 15 deg for the 0.5-scale model were examined. Comparisons of results by heat-transfer gages, thermographic phosphor, and surface thermocouple heat-transfer measurement techniques are presented. Color photographs showing heat-transfer-rate contours measured by the thermographic phosphor technique are included.

CONTENTS

		Page
	ABSTRACT	iii
	NOMENCLATURE	vi
I.	INTRODUCTION	1
II.	APPARATUS	
	2.1 Models	1
	2.2 Wind Tunnel	2
	2.3 Instrumentation	3
III.	PROCEDURE	
	3.1 Test Conditions and Procedure	5
	3.2 Data Reduction	6
	3.3 Data Precision	8
IV.	RESULTS AND DISCUSSION	9
V.	CONCLUSIONS	13
	REFERENCES	14

APPENDIXES

I. ILLUSTRATIONS

Figure

1.	0.25-Scale HAST Model	17
2.	0.5-Scale HAST Model	18
3.	0.25-Scale Model Dimensions and Heat Gage Locations	19
4.	0.5-Scale Model Dimensions and Heat Gage Locations	25
5.	Variation of Phosphor Brightness with Temperature for U. S. Radium Radelin®#1807 Phosphor	28
6.	Sketch of Gardon Gage and Surface Thermocouple Model Installation	29
7.	Calibration Curve for Camera 1, 0.5-Scale Model, δ_c = 5 deg, α = 0, Showing How Data Color is Related to Measured Stanton Number	30
8.	Comparisons of Measured and Color-Indicated Stanton Numbers for Randomly Selected Data	31

Figure Page

9. Comparison of a Theoretical Calculation for Stanton Number Distribution with Measurements, δ_c = 15 deg, α = 0, $Re_\ell \approx 21 \times 10^6$, M_∞ = 4.03 32

10. Top View of 0.25-Scale Model Showing Heating Patterns, δ_c = 15 deg, α = 0, $Re_\ell \approx 21 \times 10^6$, M_∞ = 4.03 33

11. Bottom-Side View of 0.25-Scale Model Showing Heating Patterns, δ_c = 15 deg, α = 4 deg, $Re_\ell \approx 21 \times 10^6$, M_∞ = 4.03 34

12. Photograph of Datacolor Analysis of Phosphor Brightness Variations Using Ten Color Increments, δ_c = 15 deg, α = 4 deg, $Re_\ell \approx 21 \times 10^6$, M_∞ = 4.03 35

13. Stanton Number Distribution Along a Line on Model Left Side 60 deg from Most Windward Streamline on 0.25-Scale Model, δ_c = 15 deg, α = 4 deg, $Re_\ell \approx 21 \times 10^6$, M_∞ = 4.03 39

14. Photographs of the 0.5-Scale Model at Several Angles of Attack Showing the Regions of Most Intense Interference Heating, $Re_\ell \approx 21 \times 10^6$, M_∞ = 4.03 40

15. Phtotgraph of Datacolor Analysis of Phosphor Brightness Variations Using Ten Color Increments, δ_c = 5 deg, α = 0, $Re_\ell \approx 21 \times 10^6$, M_∞ = 4.03 41

16. Stanton Number Distributions Along Two Meridians of the 0.5-Scale Model Showing Variations in Heating Rate with Angle of Attack, $Re_\ell \approx 21 \times 10^6$, M_∞ = 4.03 43

II. TABLE

I. Test Summary 45

NOMENCLATURE

c_p	Air specific heat, 0.248 Btu/lbm-°R
h	Heat-transfer coefficient, Btu/ft^2-sec-°R
L	Length of antennae domes, in.

ℓ	Model length: 50 in. for both 0.25- and 0.5-scale models
M_∞	Free-stream Mach number
p_O	Tunnel stilling chamber pressure, psia
$\dot{q}$	Heat-transfer rate, Btu/ft^2-sec
Re_ℓ	Free-stream Reynolds number based on model length
STA	Model axial station, distance from STA 0 (model nose), in.
St	Stanton number
T_{aw}	Adiabatic wall temperature, °R
T_g	Heat gage edge temperature, °R
T_O	Tunnel stilling chamber temperature, °R
V_∞	Free-stream velocity, ft/sec
α	Angle of attack, deg
δ_c	Canard deflection angle (positive for trailing edge down), deg
ρ_∞	Free-stream density, slugs/ft^3
ϕ	Model roll angle, deg

SECTION I
INTRODUCTION

The purpose of this investigation was to obtain aerodynamic heating distributions on the High Altitude Supersonic Target (HAST) configuration being developed for the Air Force Armament Test Laboratory (AFATL), Eglin Air Force Base, Florida. The Air Force Flight Dynamics Laboratory (AFFDL), Wright-Patterson Air Force Base, Ohio, planned the test program for AFATL. Of particular interest in the program was the interference heating generated by antennae domes, pitot probes, and launch pins.

The tests were conducted in the von Kármán Gas Dynamics Facility (VKF) 40-inch Supersonic Wind Tunnel (A) at Mach number 4 and a model length Reynolds number of about 21×10^6. Two models were used in the test program - a 0.25-scale model of the complete configuration and a 0.5-scale model of the front half of the configuration. The 0.25-scale model was tested at angles of attack from -8 to 12 deg, with canard deflection angles of 0 and 15 deg; the 0.5-scale model was tested for angles of attack from 0 to 12 deg, with canard deflection angles of 0, 5, 10, and 15 deg. Force tests done at AEDC with the HAST configuration (sans antennae, launch pins, etc.) have been reported in Refs. 1 and 2.

The current tests involved the use of thermographic phosphors - a relatively new heat-transfer testing technique, along with Gardon-gage-type, direct heat-transfer-rate measurements. Previous tests using this technique are reported in Refs. 3, 4, and 5.

SECTION II
APPARATUS

2.1 MODELS

The two test models were a 0.25-scale model of the complete configuration (Fig. 1, Appendix I) and a 0.5-scale model of the front half of the configuration (Fig. 2). Both models were 50 in. long, and diameters for the 0.25- and 0.5-scale models, respectively, were 3.25 and 6.50 in. Model details, including instrumentation locations, are shown in Figs. 3 and 4.

The models were constructed from Material G®, a proprietary unfilled epoxy, by Grumman Aerospace Corporation. This material was used because of its low thermal conductivity, which was needed for the proper degree of temperature sensitivity. The epoxy was molded around a 2.25-in.-diam steel tube with a 1.63-in. ID that functioned as the model mounting sting. Each model has 25 AEDC/VKF-supplied Gardon-type heat-transfer gages (Figs. 3 and 4 and Ref. 6), and, about 0.125 in. ahead of each gage location, a Chromel-Alumel® surface thermocouple was molded into the model. The 0.5-scale model had four surface pressure orifices located in the symmetrical plane opposite the nonfunctioning pitot probe (Fig. 4a). Each model had a Material G and a metal set of canards. As anticipated, the Material G canards failed under aerodynamic loads during high-angle-of-attack testing and had to be replaced with the metal canards.

Model configuration variables were limited to canard deflections of 0 and 15 deg for the 0.25-scale model and 0, 5, 10, and 15 deg (positive is trailing edge down) for the 0.5-scale configuration. Grit roughness (see Table I, Appendix II, for sizes) was applied on the nose of each model and on the right wing upper and lower leading edges of the 0.25-scale model to ensure a turbulent boundary layer on these surfaces.

2.2 WIND TUNNEL

Tunnel A is a continuous, closed-circuit, variable density wind tunnel with an automatically driven flexible-plate-type nozzle and a 40- by 40-in. test section. The tunnel can be operated at Mach numbers from 1.5 to 6 at maximum stagnation pressures from 29 to 200 psia, respectively, and stagnation temperatures up to 750°R (M_∞ = 6). Minimum stagnation pressures range from about one-tenth to one-twentieth of the maximum pressure at each Mach number.

The models can be injected into the tunnel for a test run and then retracted for model cooling or modifications without interrupting the tunnel flow. A description of the tunnel and airflow calibration information may be found in Ref. 7.

2.3 INSTRUMENTATION

2.3.1 Thermographic Phosphor Paint

Thermographic phosphorescence is the emission of luminescent light having temperature-dependent intensity that decreases exponentially with increasing temperature. The paint phosphorescence is activated by ultraviolet (UV) light, and the intensity of emission depends on the properties of the particular phosphorescent paint and the energy of the activating ultraviolet light, as well as the temperature. A plot of the emission brightness for the phosphor used in this test is given in Fig. 5 as a function of phosphor temperature; the intensity of the ultraviolet lights for this was nominally two ultraviolet light units (200 $\mu w/cm^2$).

The technique for obtaining the model surface heating patterns at the desired test conditions consists of photographing the painted model surface and measuring the optical density (brightness) of the recorded image. The measured density is related to the model surface temperature, which can be related to the surface aerodynamic heat-transfer coefficient.

A simple method of determining this proportionality is to measure the surface temperature and heat-transfer rate at several model locations at the same time the paint pictures are being made. These measurements are used to establish reference heat-transfer coefficients for the paint data, from which it is possible to deduce the detailed heating distribution over the model. The instrumentation used for the surface temperature and heat-transfer measurements is discussed in the following sections. A more complete discussion of the phosphorescent paint techniques is reported in Ref. 3.

The model phosphorescence photographs were obtained using Beattie-Coleman Varitron® 70-mm sequence cameras set at f/5.6 and 0.5-sec exposure, and Eastman Kodak Tri-X Pan® film, developed using the Eastman Kodak Versamat® process.

2.3.2 Heat-Transfer Gages and Surface Thermocouples

The surface heat-transfer rates at several locations on the models (see Section 2.1) were measured with a high sensitivity gage that operates on the Gardon gage principle (Ref. 6) but has an order of magnitude higher sensitivity. This gage was developed at AEDC/VKF for use

in continuous wind tunnels. The gages were installed in the model surface, as shown schematically in Fig. 6. Most of the gages were nominally 0.25-in. OD by 0.38 in. deep; however, some 0.187-in.-OD gages were used to accommodate greater model curvature near the 0.25-scale model nose. Gage location, size, and sensing foil thickness are indicated on the model sketches in Figs. 3 and 4.

The gage aerodynamic heat-transfer rate was determined by the expression

$$\dot{q} = C \cdot E(t)$$

where $\dot{q}$ is the time-dependent heat-transfer rate, C is the gage scale factor, and E(t) is the measured voltage as a function of time. The scale factor, C, was determined by experimental calibration using a radiant heat source. Calibration was obtained by exposing one or more test transducers and heat-transfer standards to the same incident heat flux and measuring the output from each simultaneously. The heat-transfer standards have been checked by two independent organizations and found to agree within ±4 percent. Accuracy of the test calibrations is estimated to be within ±5 percent, and gage repeatability and linearity are estimated to have been within ±3 percent.

Internal to each heat gage, a copper-constantan thermocouple was installed to monitor the gage edge temperature. The temperature indicated from this thermocouple was used with the measured heat-transfer rate to compute the aerodynamic heat-transfer coefficient at the gage location.

The surface thermocouples were molded into the model at fabrication (see Fig. 6) and were made of #30 gage Chromel-Alumel wire. Accuracy of the thermocouple measurements is estimated to be ±2°R or ±0.5 percent of the measurement, whichever is greater.

2.3.3 Pressure

The four surface pressures on the 0.5-scale model were measured with 15-psid precision pressure balance-type transducers. The associated servoamplifiers may be calibrated to provide full-scale output for ranges of 15, 5, and 1 psid, using expanded sensitivity for the 5- and 1-psid ranges. The transducers were fixed on the 5-psid range for this test. Based on repeat calibrations, the estimated precision was ±0.02 psi.

SECTION III
PROCEDURE

3.1 TEST CONDITIONS AND PROCEDURE

3.1.1 Test Conditions

The configuration variables examined in this test program were canard deflection angle for both models and the turbine pump inlet configuration on the 0.25-scale model, plugged or unplugged. The table in Appendix II contains a complete list of the model test attitudes and conditions for both configurations. A summary of the tunnel operating conditions is presented as follows:

M_∞	p_o, psia	T_o, °R	ρ_∞, slugs/ft^3	V_∞, ft/sec	$Re_\ell \times 10^{-6}$
4.03	73	660	2.52×10^{-4}	2460	20.7

3.1.2 Test Procedure

In order to provide the best possible reflective coating for the phosphor emission, the models were painted white before the phosphors were applied. They were then sprayed with the phosphor mixture under ultraviolet light to obtain a thin, uniform coat.

Because of possible nonuniformities in either the phosphor coating or the incident ultraviolet light (for example, shadows caused by model geometry), pretest pictures of both models were obtained in the test section under the same conditions (but without the tunnel running) that existed for the test pictures. By subtracting the measured optical density of the pretest picture from the test picture, the influence of these nonuniformities was eliminated from the final results.

The test sequence consisted of injecting the model, translating it forward to the test section, and taking at least three photographs of the model at 3-sec intervals. The model remained in this position about 12 sec, and total elapsed time from initial model exposure to the flow to beginning of retraction was about 26 sec. The model was cooled to about 75 to 80°F, the gage-edge temperature and the model surface temperature being monitored during the cooling cycle to ensure a uniform temperature distribution before a subsequent test injection.

The outputs from the heat-rate gages, gage-edge temperature thermocouples, and surface thermocouples (and the four surface pressures on the 0.5-scale model) were recorded continuously from before the model injection until the beginning of the retract cycle. The recordings were made on magnetic tape with a Beckman 210 analog-to-digital converter, each channel being sampled every 0.05 sec during the recording interval. Indicate bits were put on the recording to mark the time sequence of events such as model arrival on centerline, model arrival in test section, and time during which photographs were being taken. Because the exposure time for the pictures was 0.5 sec, the average of the nominally ten readings recorded for each channel during that interval was used in the data reduction.

Because of the large model size, two cameras were required to photograph the complete model (one for the front half and the other for the rear). A total of four cameras was used (two on the tunnel operating side and two on the nonoperating side) so that photographs were obtained of either the model top and bottom views or both side views simultaneously. The top and bottom or both side views were selected by changing the model roll about the tunnel axis of symmetry; the tunnel roll mechanism was kept at zero pitch angle, and a variable prebend adapter (±12 deg in 2-deg increments) was used to set the desired model angle of attack.

3.2 DATA REDUCTION

Data reduction of the phosphor paint patterns was accomplished using a Datacolor 703-32® analyzer. The Datacolor system uses a black-and-white television (TV) camera to produce a standard TV signal, or image, of the test picture. A digital video processor analyzes the shades of gray in the TV image and classifies them into up to 32 different increments of shades of gray (ten increments were used in the present analysis). A different color is assigned to each increment, and the appropriate color TV signal for each color is generated by the digital processor. The sum of these signals is displayed on a color monitor unit. The colors on the monitor correspond incrementally to the shades of gray in the original black-and-white picture. System linearity was monitored by observing the system output of a continuous density wedge on an oscilloscope.

The black-and-white picture that is analyzed is a composite of the test picture negative and a positive copy (with gamma = 1.0) of the

pretest picture negative. The superposition of these two pictures yields the difference in density between them. This difference in film density represents the change in temperature between the test condition and the pretest condition. Moreover, neglecting the transient heating that occurs during injection through the tunnel boundary layer, the contours of constant film density (constant surface temperature) denote areas of constant aerodynamic heat-transfer coefficient.

The measured heat-transfer rates and the associated gage-edge temperature were used to compute the aerodynamic heat-transfer coefficient at the gage location by the equation

$$h = \frac{\dot{q}}{(T_{aw} - T_g)} \tag{1}$$

and the local Stanton number was computed as

$$St = \frac{h}{\rho_\infty V_\infty c_p} \tag{2}$$

where T_g was the gage-edge temperature, $\dot{q}$ was the heat gage heating rate, and T_{aw} was the adiabatic recovery temperature; c_p was taken as 0.248 Btu/lbm-°R. Experimentally, since T_{aw} could be either the laminar or turbulent adiabatic wall temperature, h and St for both conditions were computed and analyzed for best correlation.

Because grit roughness had been applied to the models, the correlation was attempted first by plotting the gage turbulent Stanton number versus color. One test without grit was made with the 0.25-scale model at zero angle of attack; much-reduced heat-transfer rates were observed, supporting the effectiveness of the grit roughness in producing a turbulent boundary layer.

The procedure used to obtain the relation between the colors displayed on the Datacolor system and the measured heat-transfer coefficients in depicted in Fig. 7. This plot of color versus Stanton number was obtained by observing the location of a particular gage in the color photograph and assigning the measured Stanton number to the color at that location. A fairing of these "data points," then, provides a calibration for the color data. Thus, the Stanton number distribution over the visible portion of the model can be determined from the colors displayed. Some caution should be exercised in the extrapolation of this fairing, since several factors can influence the relation between surface

temperature (color) and Stanton number. A calibration such as that shown in Fig. 7 is provided for each photograph because the Datacolor system sensitivity is adjusted to provide optimum coverage of each photograph.

In some cases, the Stanton number based on the gage data did not appear to correlate with the color data as well as expected. In these cases the temperature-time history of the surface thermocouple located near the gage was used with the theoretical solution to the heat conduction equation for a semi-infinite solid. This provided a Stanton number independent of the gage measurement. Several of these points are shown in Fig. 7 and are also presented in subsequent data figures. Almost without exception, the Stanton numbers indicated from the surface thermocouples improved or substantiated the Stanton number-color data correlation.

3.3 DATA PRECISION

Uncertainites (bands which include 95 percent of the calibration data) in the basic tunnel parameters, p_o, T_o, and M_∞, were estimated from repeat calibrations of the instrumentation and from the repeatability and uniformity of the test section flow during tunnel calibrations. Using the Taylor series method of error propagation, the authors then used these uncertainties to estimate uncertainties to estimate uncertainties in other free-stream properties, all of which are listed as follows:

Uncertainty (±), percent					
M_∞	p_o	T_o	ρ_∞	V_∞	Re_ℓ
0.5	0.5	0.2	2.0	0.2	1.2

Measurements of model attitude in pitch and roll are precise within ±0.05 and ±0.1 deg, respectively, based on repeat calibrations and measurements.

The estimated precision of the heat gage and thermocouple measurements, as well as the computed Stanton number and heat-transfer coefficients, is tabulated below:

Parameter	Uncertainty (±), percent
Heat-transfer rate, $\dot{q}$	8.0
Surface and gage-edge temperature	0.5
Heat-transfer coefficient, h	13.0
Stanton number, St	13.0

The precision of the Datacolor system has been described by its manufacturer as follows: The light table to illuminate the test picture has a light intensity variation of less than ±5 percent at a light intensity of more than 1000 foot-candles, the video signal from the TV camera is converted to a true logarithmic density scale over the range from 0 to 2 within ±3 percent of full scale, and the color shading on the color monitor corresponds to a density change of less than 0.05 (change in light transmission of 10 percent) over the center area of the picture within a circle whose diameter is 0.8 of the picture height. On the average, the density range of all the superimposed test pictures was 0.75, so the square root of the sum-of-the-squares summation of all these contributing errors, along with the 8-percent uncertainty of the measured Stanton number, yields an estimated uncertainty for the color-indicated Stanton number to be ±17 percent.

To check how realistic this estimate is, a random sampling (117 points) of the data was made comparing the Stanton number based on a measured heat-transfer rate and the Stanton number indicated by the color photographs. The results are shown in Fig. 8. Figure 8a shows the ratio of gage-measured Stanton number to color Stanton number versus color Stanton number, and Fig. 8b is a normal distribution curve of the frequency of ratios occuring within a 0.04 band width plotted against the Stanton number ratio. The mean of the sampling was determined to be 1.018, or 1.8 percent above exact agreement, and the standard deviation of this distribution was computed to be 0.101, which means that on a probability basis 68 percent of all the data were within ±10 percent of exact agreement. Two standard deviations (±20 percent) would include 95 percent of the data.

SECTION IV
RESULTS AND DISCUSSION

Although good correlation between the color-indicated Stanton numbers and those from the Gardon gages or surface thermocouples has been demonstrated (Fig. 8), the validity of these data remains to be

established in relation to either other measurements or theoretical calculations. No other heat-transfer measurements are known to be available for this configuration; hence, only theoretical calculations can be used in the validation.

A comparison of the measured Stanton numbers with the distribution computed for the HAST 0.25-scale model using the theory developed in Ref. 8 is presented in Fig. 9 for the zero angle-of-attack case. In general, the trend of the measured data agrees very well with the theoretical distribution, and to this extent the measurements are considered validated. The indicated 30-percent difference between a fairing of the measurements and the theoretical distribution is thought to be caused by the fact that the model wall temperature was within 10 percent of the estimated adiabatic wall temperature, so that small differences between the computed and actual boundary-layer temperature profiles could be magnified significantly in terms of heat-transfer rates. Moreover, a 2-percent increase in the estimated adiabatic wall temperature would result in a 21-percent reduction in the measured Stanton number.

The measurements for the 0.5-scale model shown in Fig. 9 have been increased by the factor 1.15 for comparison with the results for the 0.25-scale model. This factor was determined by considering the two-fold increase of the local Reynolds number for the 0.5-scale model. This difference, incorporated into the classical turbulent skin-friction variation with Reynolds number, would suggest a $(2)^{0.2} = 1.15$ difference in skin friction and, through Reynolds analogy, in heat-transfer rate for the two models. The good agreement obtained appears to confirm this consideration.

Also shown in Fig. 9 are the Stanton numbers obtained from the surface thermocouple/semi-infinite slab theory technique to illustrate the good agreement with the Gardon gages. Because in some positions the Gardon gages were inoperative, the only measurements available were those from the thermocouples.

Because of the radomes and other protuberances on the models, only those measurements least likely to have interference effects were used for the comparison in Fig. 9. The gages along the meridian 45 deg from the model top (see Fig. 10) were selected. In Fig. 9, all the measurements from these gages appear to be fairly interference-free except those at STA 24.25. Figure 10 presents a photograph of the heating patterns on the 0.25-scale model top surfaces, and examination of the patterns around gages 64 (STA 24.25) and 84 (STA 32.50) shows a

shock impingement pattern close to each gage. It appears that the shock impingement crossed over gage 64, causing the noticeable increase of the Stanton number shown at that location, whereas the one around gage 84 appears to be more diffuse and crossed behind the gage, thus having little or no effect on the measurement.

An illustration of the application of the Datacolor analysis technique is next considered to show its capabilities. Presented in Fig. 11 is a phosphor data photograph of the model in the attitude selected for analysis. Also shown in Fig. 11 is the meridan along which the Stanton number distribution was evaluated. This meridian was chosen to provide comparisons with the largest possible number of gage measurements.

Photographs of the Datacolor system rendition of the pictures shown in Fig. 11 are presented in Figs. 12a and b for the model front and rear halves, respectively. These photographs clearly illustrate the basic advantages of the Datacolor analysis, which are the vivid contouring and quantification of the heating patterns. The peak heating regions caused by shock interaction in the canard area are readily identified by the yellow and light-blue areas. Note that color identification bars are included with each photograph to ensure accurate correlation of colors and heating rates. Some difficulty in identifying model geometric details in the color photograph is normally experienced, and correlation with the black-and-white photograph (Fig. 11) is generally required for orientation. High heating rates (light green-green) are also observed on the aft portion of the vehicle (Fig. 12b), on the fin leading edges, and on the antenna dome located at the center of the fin. The location of the meridian selected for analysis in Fig. 11 may be determined from the gages (shown as black spots). Some areas in the photographs are excluded from the analysis because of marginal lighting on the model nose and conduction effects on the thin sections of the canards and the flow-through turbine inlet.

The technique for determining the Stanton number distribution along the selected meridian was to note the points on the meridian where color changes occurred. At these points the Stanton number was determined from the calibration curve (similar to the one shown in Fig. 7), and the locations were measured from a known position. Shown in Fig. 13 is the plot of Stanton number versus model axial station for the selected meridian (see Fig. 11) with the noted color-change points indicated. Also, the range of Stanton number for each color is shown along the dividing line between the two pictures. The distribution was obtained by fairing

these points; the relative maximums and minimums shown were obtained from consideration of the largest and smallest value of Stanton number corresponding to a particular color. For example, the green streak which occurs downstream of gage 42 (the third one back from the model nose) in Fig. 12a may have a maximum heating rate less than the value indicated at axial STA 14.0, which corresponds to the maximum value for the green color; but to avoid underestimating the actual value, the maximum is shown.

The peaks shown at STA 26.8, 28.4, and 34.7 in Fig. 13 can be clearly seen in Fig. 11 (points 1, 2, and 3) and in Fig. 12b by close inspection. The magnitude of the peaks was determined by the maximum value for the prepresented color. Generally, the gage measurements indicate good agreement with the distribution, and, where possible, good agreement is obtained between the gage and surface thermocouple measurements. Exception to this are shown at STA 24 and 32.5. Again referring to Fig. 11, a hot streak that is clearly visible upstream appears to be directed toward gage 62 (STA 24.25), thereby possibly causing the higher heating rates observed at that station. The difference between the two measurements at STA 32.5 is clearly a case of a shock impingement crossing the thermocouple but missing the gage, as can readily be seen in Fig. 11.

The primary test objective of locating the areas of most intense interference heating was readily accomplished by observation of the models during the test. Presented in Fig. 14 are photographs that show the areas of maximum interference heating that were observed on the 0.5-scale model at three typical angles of attack. Heating around the launch pins on the 0.25-scale model (see Fig. 10) appeared just as intense, but over a much-reduced area. Shown also in Fig. 14 are the selected meridians along which the Stanton number distributions are to be determined. These meridians are located with respect to the bottom line of symmetry at 15 and 45 deg.

Shown in Fig. 15 is a photograph of the Datacolor results for the zero angle-of-attack case. Below the pitot probe in this photograph, the light-blue area encircled by light green indicates the increased heating caused by shock interaction between the probe and forebody rib. Displayed in yellow, the high heating area between the probe and antenna dome is very distinct. The narrow color bands just ahead of this region denote the high temperature gradient associated with this area. The aforementioned regions (on either side of the pitot probe) were observed to have the most pronounced interference heating.

Because of a slight overexposure of the tare picture, a shadow of the pitot probe is apparent in the lavender color region. When these results were plotted, this effect was compenstaed for by shifting the indicated color-change points down a half color on the calibration curve in determining the Stanton number distribution through the shadowed region between the pitot probe and the antenna dome. It was not necessary to shift the color-change points in other areas.

Presented in Fig. 16 are the Stanton number distributions determined by the Datacolor technique for the 45- and 15-deg meridians noted earlier. Comparing Figs. 16a and b reveals that the most intense interference heating occurred at zero angle of attack in the region between the pitot probe and the antenna dome (Fig. 16a, STA 18). The magnitude of the increased heating rate in this region was about 3.0 times the undisturbed heating rate presented in Fig. 9. The peak in this interference region decreased significantly with angle of attack as indicated by the 8- and 12-deg distributions. The 4-deg results have been omitted for clarity because the distribution in the peak heating region was almost identical to that for the 8-deg case. The peak heating along the 15-deg meridian (Fig. 16b) apparently caused by the interaction between the shock off of the pitot probe with that of the forebody rib changed very little with angle of attack. It should be noted, however, that the breadth of its influence widened with increased angle of attack.

SECTION V
CONCLUSIONS

Heat-transfer tests were made on the High Altitude Supersonic Target (HAST) missile at Mach number 4 and a Reynolds number, based on model length, of 21×10^6. Within the limits of the test scope, the significant results were as follows:

1. The areas of most pronounced interference heating occurred between the pitot probe and the nearest antenna dome, and the greatest shock interaction occurred between the probe and the forebody rib. While the magnitude of the heating in the former area decreased noticeably with increased angle of attack, the magnitude of the heating around the forebody rib remained essentially constant, and its area of influence was spread with increased angle of attack.

2. The maximum increase in heating attributable to shock interference was observed at the zero angle-of-attack case and was about three times the noninterference level.

3. The Datacolor analysis of the thermographic phosphor data provided vivid contouring and quantification of the model heating rates.

REFERENCES

1. Jones, J. H. "Aerodynamic Characteristics of the HAST Missile at Mach Numbers 2.25, 3, and 4." AEDC-TR-72-6 (AD890591L), January 1972.

2. Carman, J. B. "Static Stability and Inlet Characteristics of the HAST Missile at Transonic Mach Numbers." AEDC-TR-71-178 (AD887776L), September 1971.

3. Matthews, R. K., Eaves, R. H., and Martindale, W. R. "Heat-Transfer and Flow-Field Tests of the McDonnell Douglas - Martin Marietta Space Shuttle Configurations." AEDC-TR- (to be published).

4. Czysz, Paul and Kendall, D. N. "Improved Methods in Wind Tunnel Technology." McDonnell Company Report No. F938, April 1968.

5. Buchanan, T. D. "High Reynolds Number Aerodynamic Test of a Delta Wing Model at Mach Number 12." AEDC-TR-70-24 (AD507776), March 1970.

6. Gardon, Robert. "An Instrument for the Direct Measurement of Intense Thermal Radiation." The Review of Scientific Instruments, Vol. 24, No. 5 (May 1953), pp. 366-370.

7. Test Facilities Handbook (Ninth Edition). "von Karman Gas Dynamics Facility, Vol. 3." Arnold Engineering Developement Center, July 1971.

8. Mayne, A. W., Jr., and Dyer, D. F. "Comparisons of Theory and Experiment for Turbulent Boundary Layers on Simple Shapes at Hypersonic Conditions." Proceedings of 1970 Heat Transfer and Fluid Mechanics Institute, pp. 168-188, Stanford University Press, 1970.

APPENDIXES

I. ILLUSTRATIONS

II. TABLE

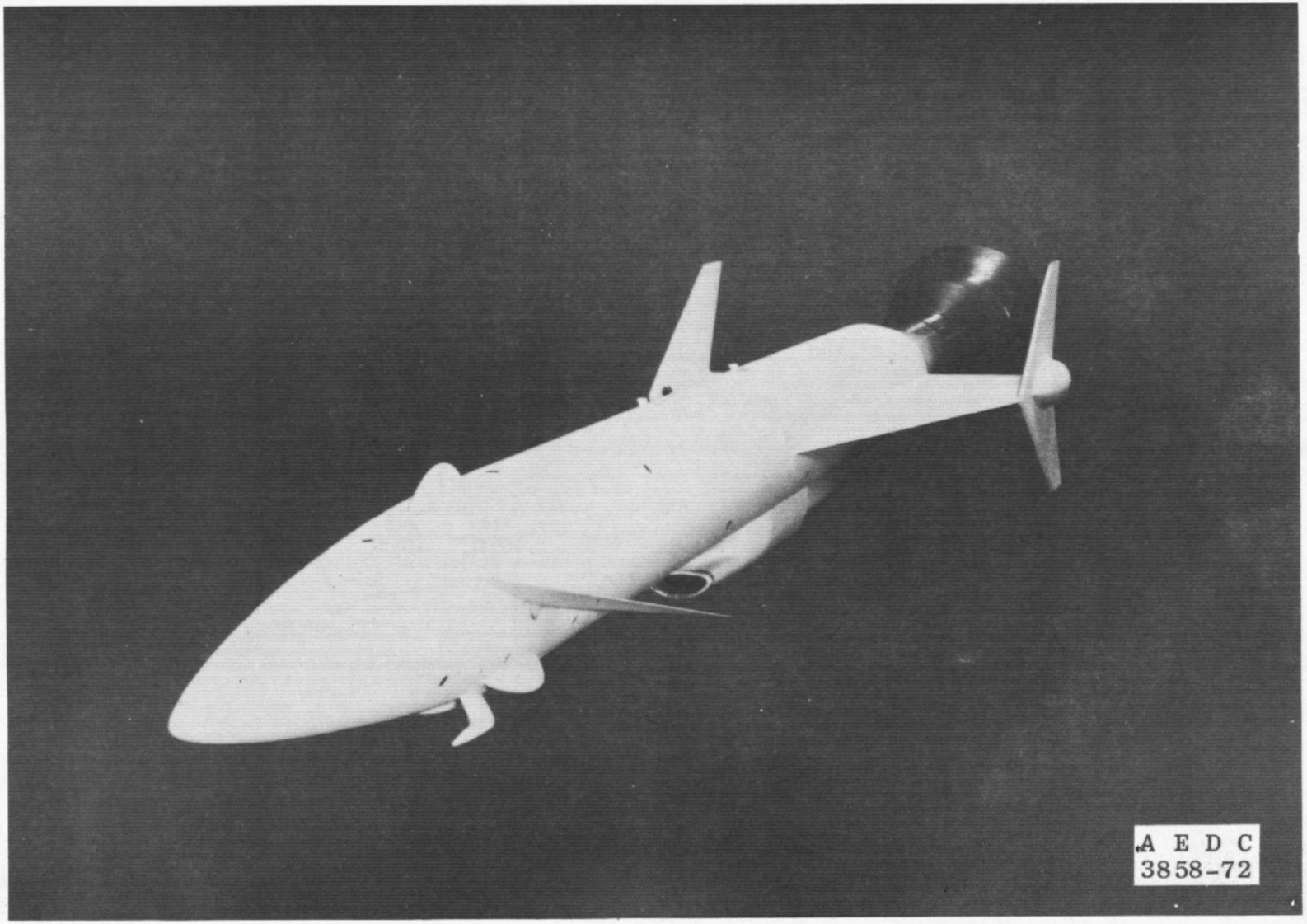

Fig. 1 0.25-Scale HAST Model

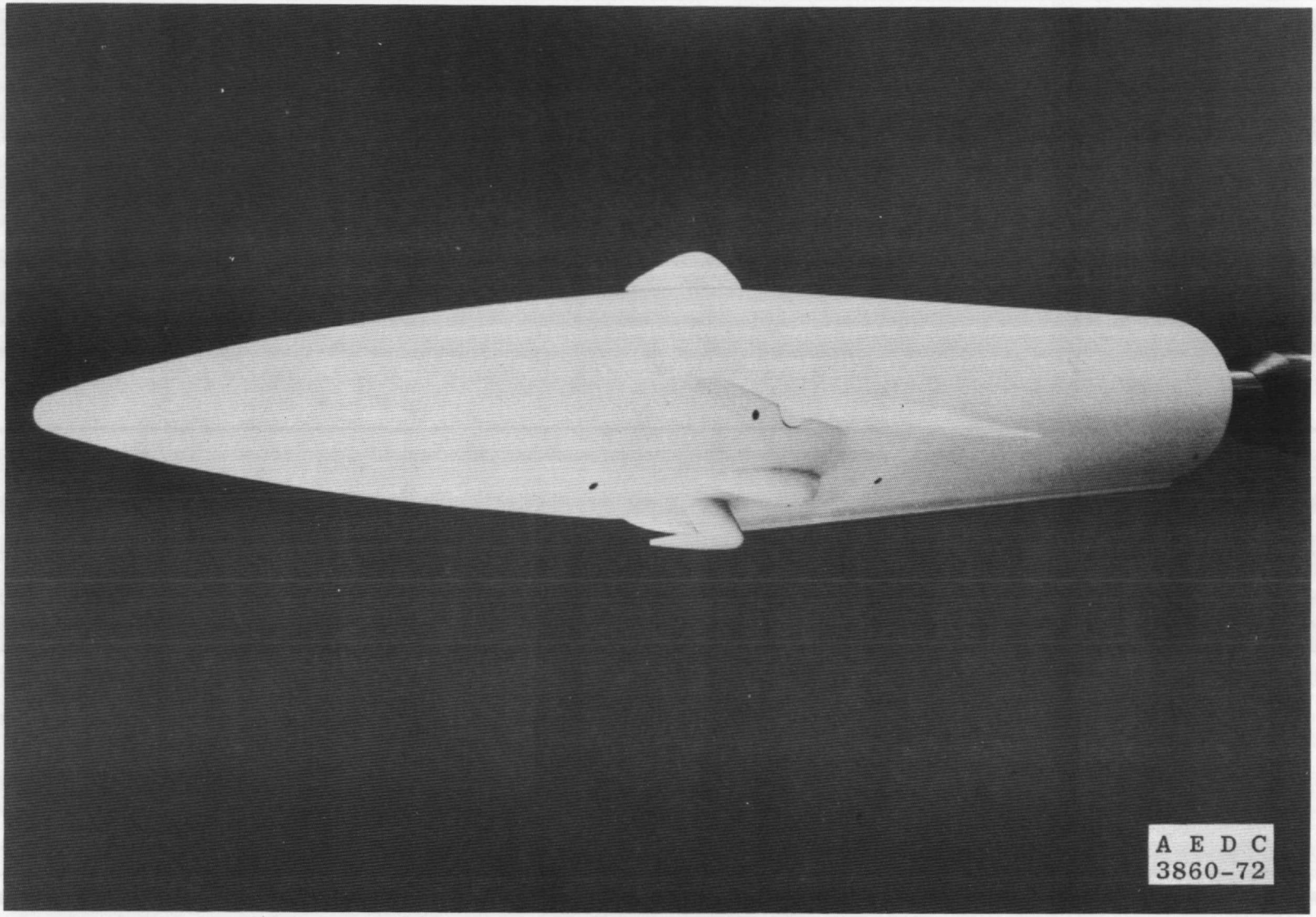

Fig. 2 0.5-Scale HAST Model

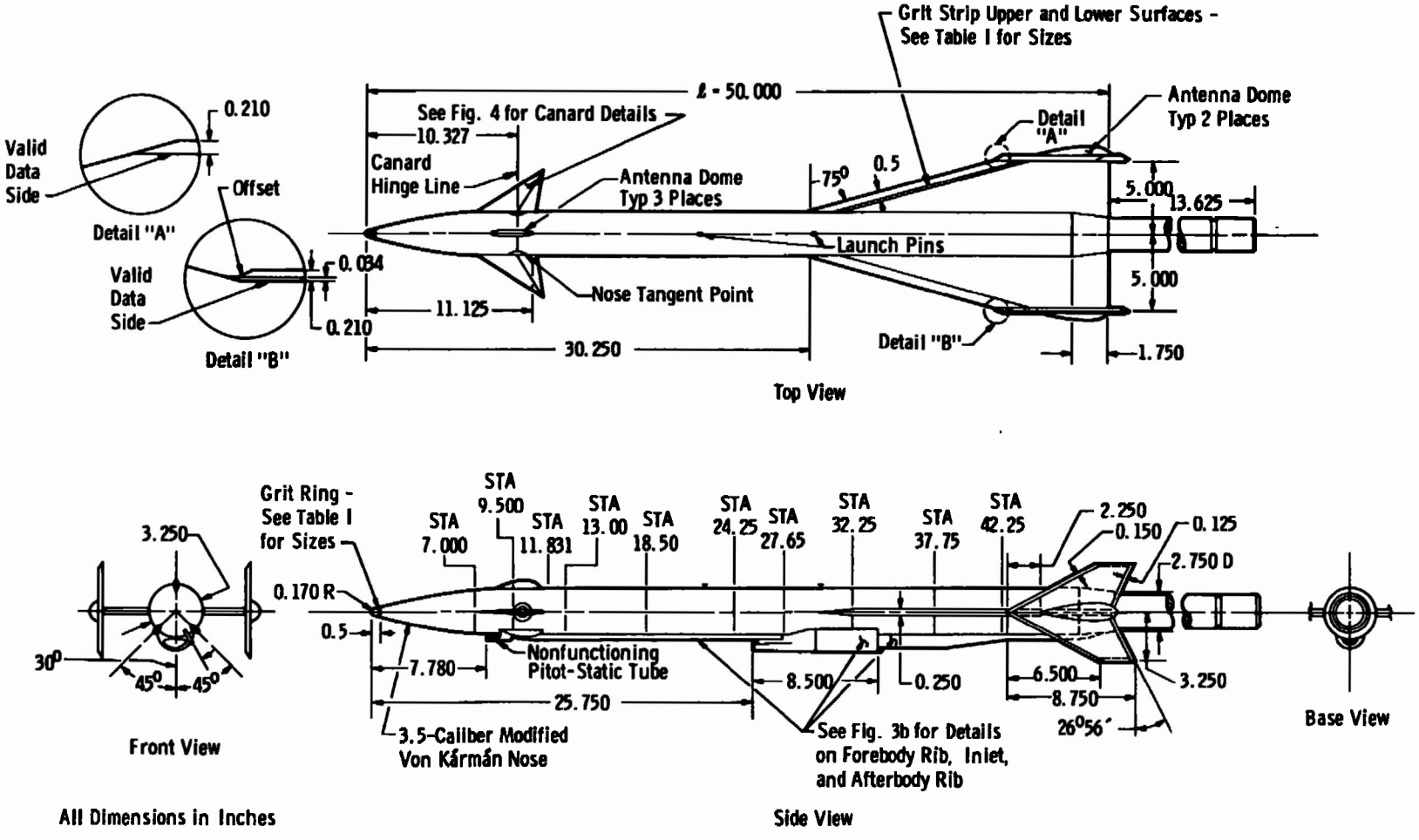

a. 0.25-Scale Model Dimensions

Fig. 3 0.25-Scale Model Dimensions and Heat Gage Locations

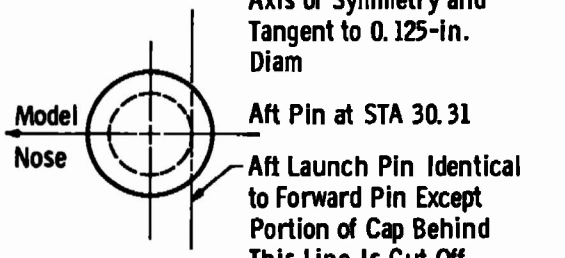

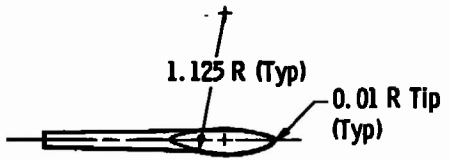

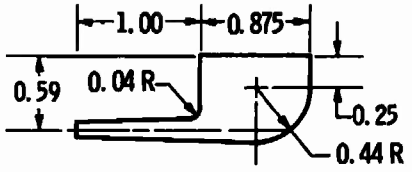

Nonfunctioning Pitot-Static Tube

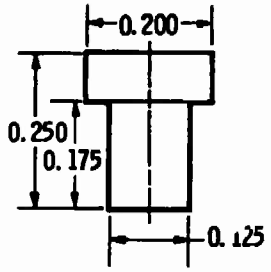

Forward Launch Pin at STA 22.2

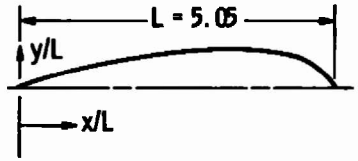

Profile of Rear Antennae Domes

Coordinates for Rear Antennae Domes

x/L	y/L
0	0
0.099	0.0356
0.198	0.0624
0.297	0.0842
0.396	0.1010
0.495	0.1139
0.594	0.1218
0.693	0.1228
0.792	0.1168
0.891	0.0971
0.921	0.0674
1.000	0

All Dimensions in Inches Unless Noted

b. Details of 0.25-Scale Model Appendages
Fig. 3 Continued

Coordinates for Forward Antennae Domes

x/L	y/L	z/L
0	0	0
0.098	0.0647	0.0392
0.196	0.1058	0.0524
0.294	0.1430	0.0608
0.392	0.1775	0.0652
0.490	0.2078	0.0662
0.588	0.2205	0.0652
0.686	0.2146	0.0608
0.784	0.1872	0.0539
0.882	0.1373	0.0397
0.980	0.0686	0.0147
1.000	0	0

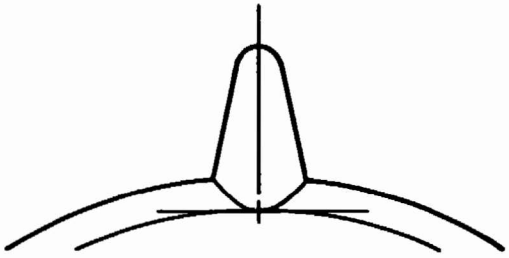

All Dimensions in Inches Unless Noted

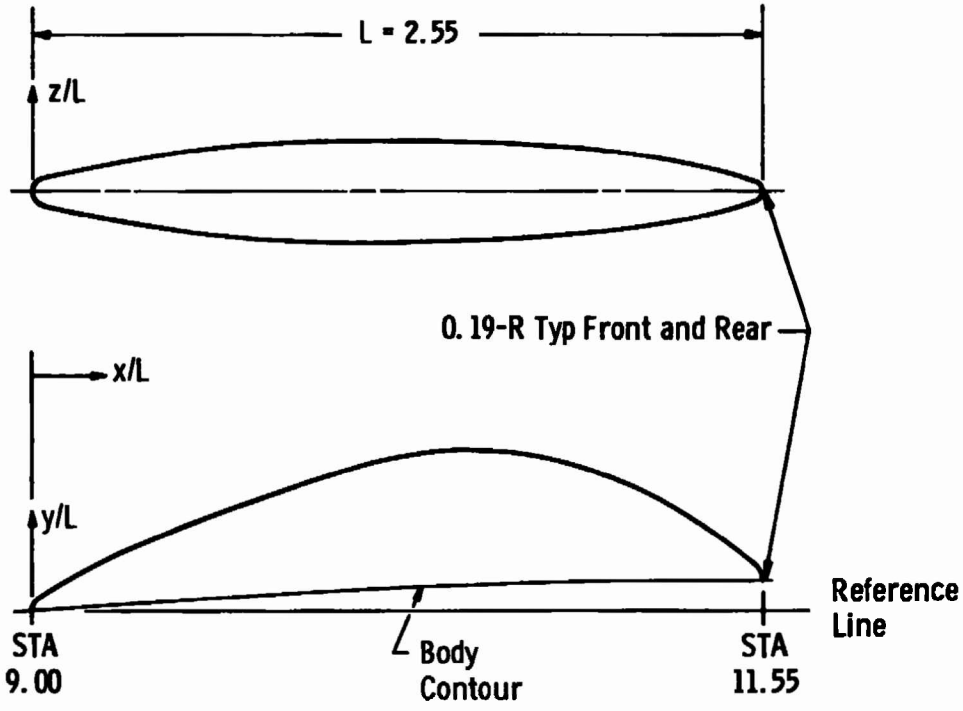

Profile of Forward Antennae Domes

b. Continued

Fig. 3 Continued

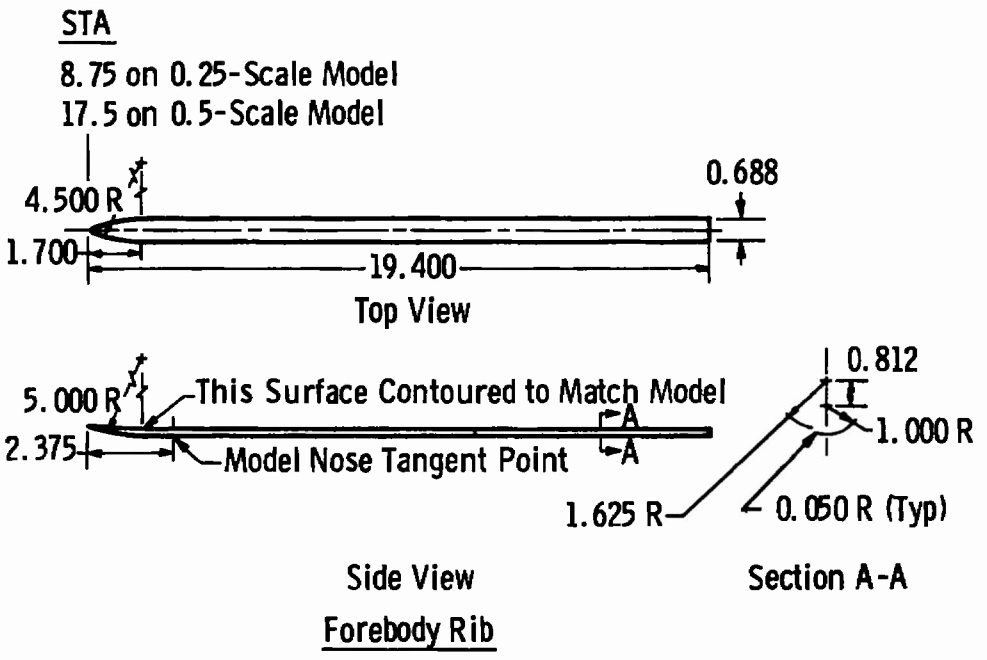

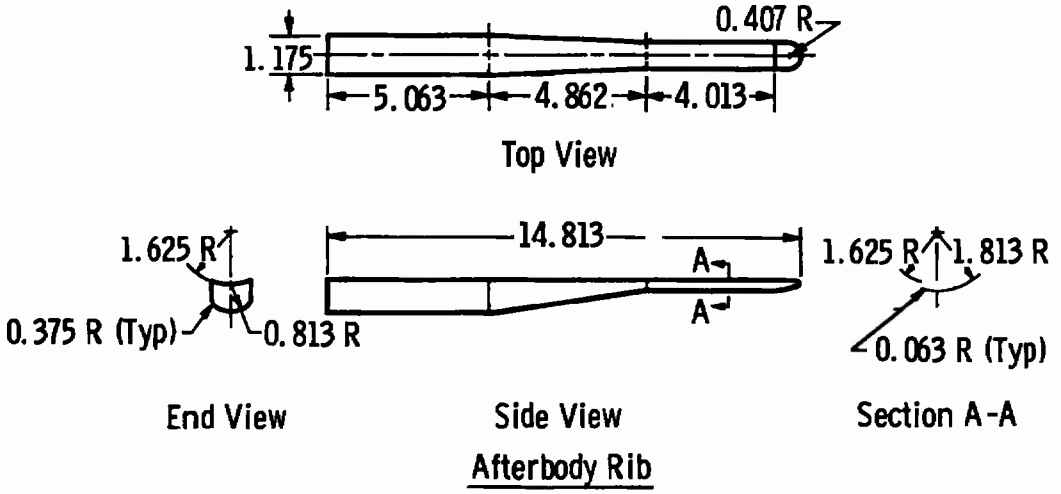

b. Continued
Fig. 3 Continued

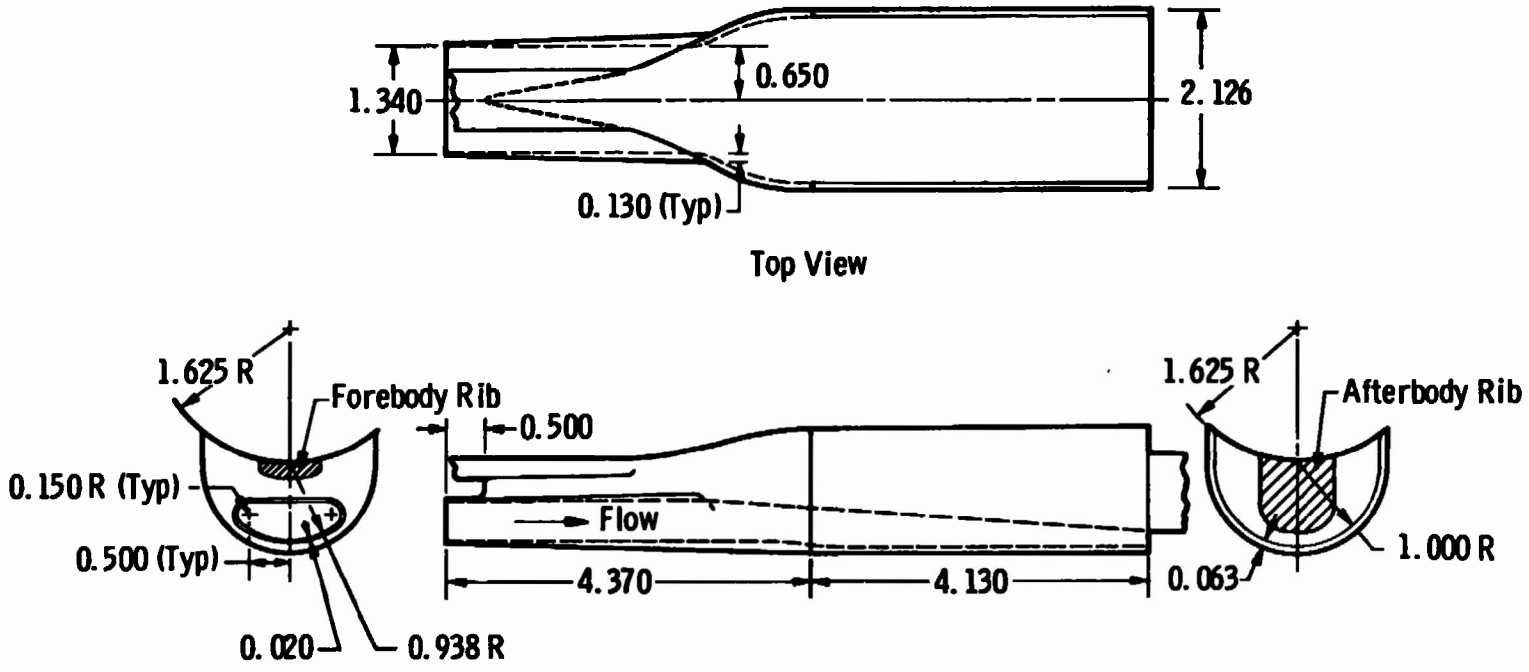

b. Concluded
Fig. 3 Continued

Gage Number	10	12	13	14	22	24	26	31	42	43	44	45	56	62	63	64	66	75	82	83	84	90	102	103	104
Foil Thickness, in.	0.002	0.002	0.002	0.002	0.001	0.001	0.001	0.002	→																0.002
Gage Diameter, in.	0.187	0.187	0.187	0.187	0.187	0.187	0.187	0.250	→																0.250

All Views Looking Forward

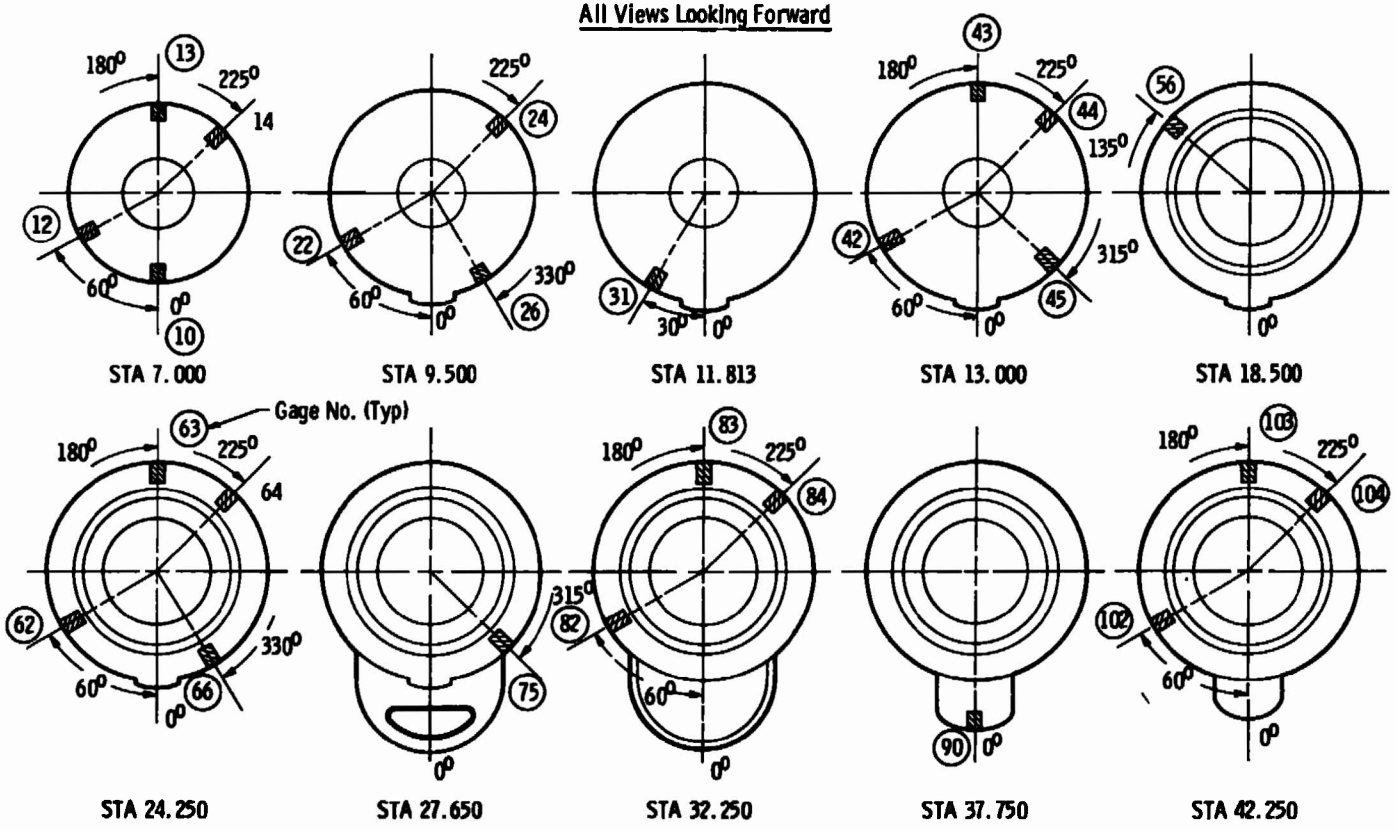

c. 0.25-Scale Model Heat Gage Locations
Fig. 3 Concluded

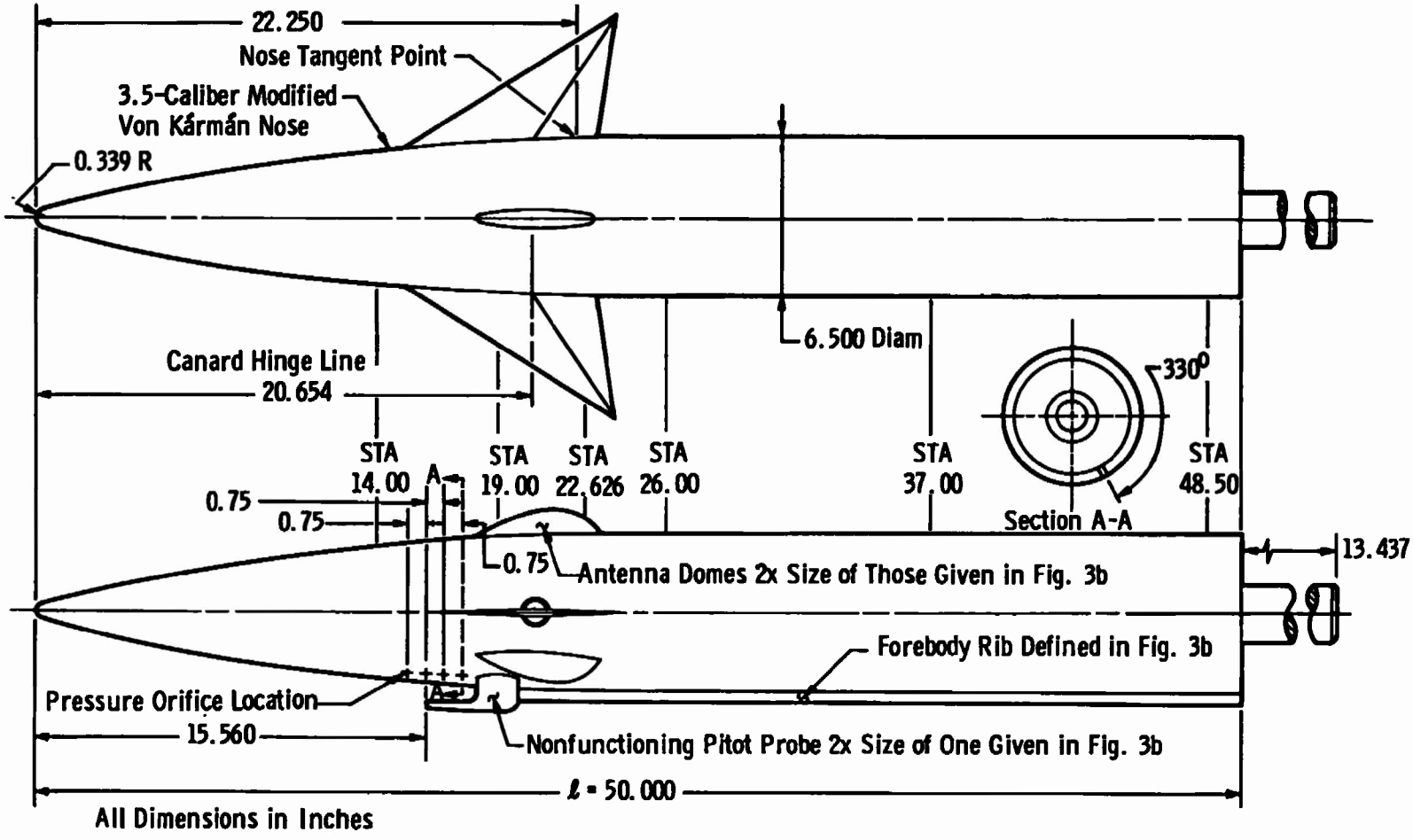

a. 0.5-Scale Model Dimensions

Fig. 4 0.5-Scale Model Dimensions and Heat Gage Locations

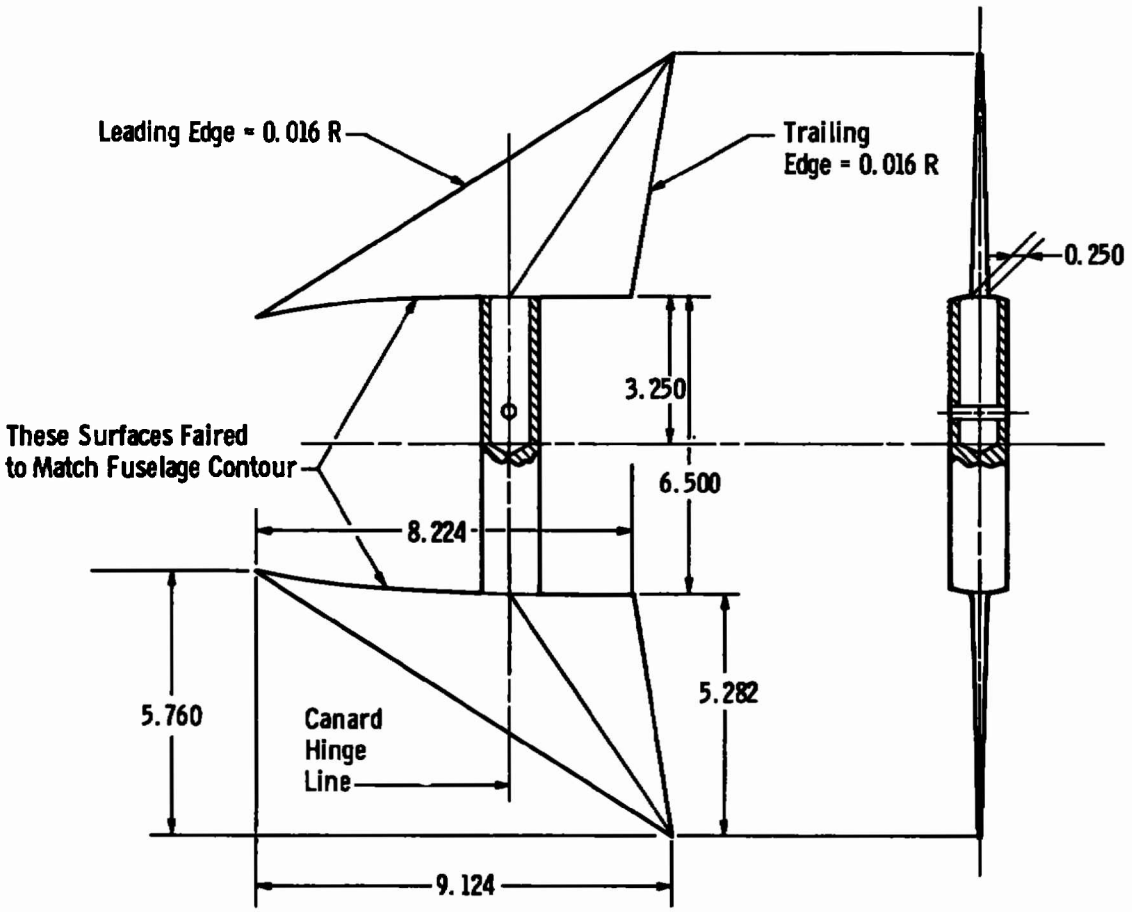

All Dimensions in Inches
Dimensions on 0.25-Scale Canards Are Half of Values Shown

b. 0.5-Scale Model Canard Dimensions
Fig. 4 Continued

Gage Number	100	120	140	150	160	230	250	260	270	300	310	370	420	430	440	450	460	470	500	540	570	620	640	650	670
Foil Thickness, in.	0.005	→	→	0.005	0.002	→	→	0.002	0.005	0.002	→	→	→	→	→	→	→	→	→	→	→	→	→	→	0.002
Gage Diameter, in.	0.250	→	→	→	→	→	→	→	→	→	→	→	→	→	→	→	→	→	→	→	→	→	→	→	0.250

All Views Looking Forward

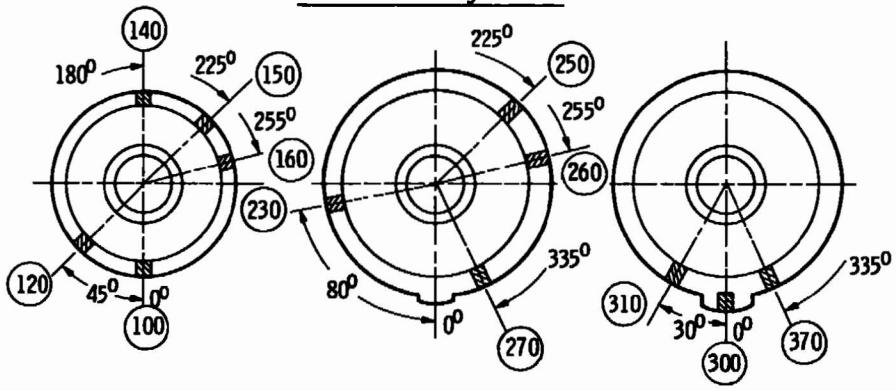

STA 14.000 STA 19.000 STA 22.626

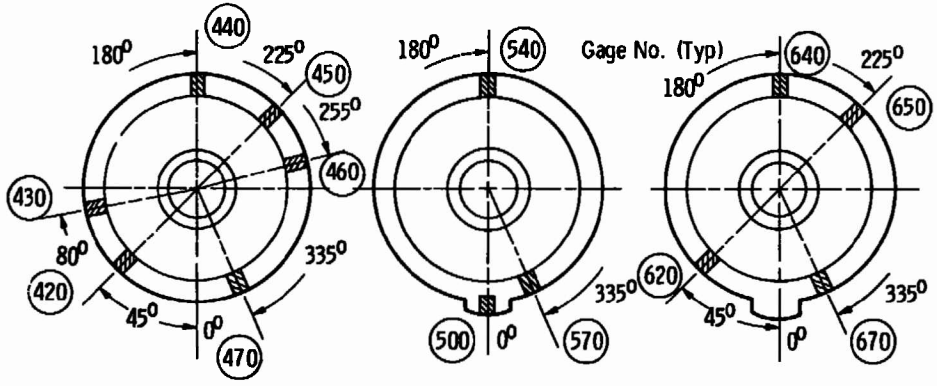

STA 26.000 STA 37.000 STA 48.500

c. 0.5-Scale Model Heat Gage Locations
Fig. 4 Concluded

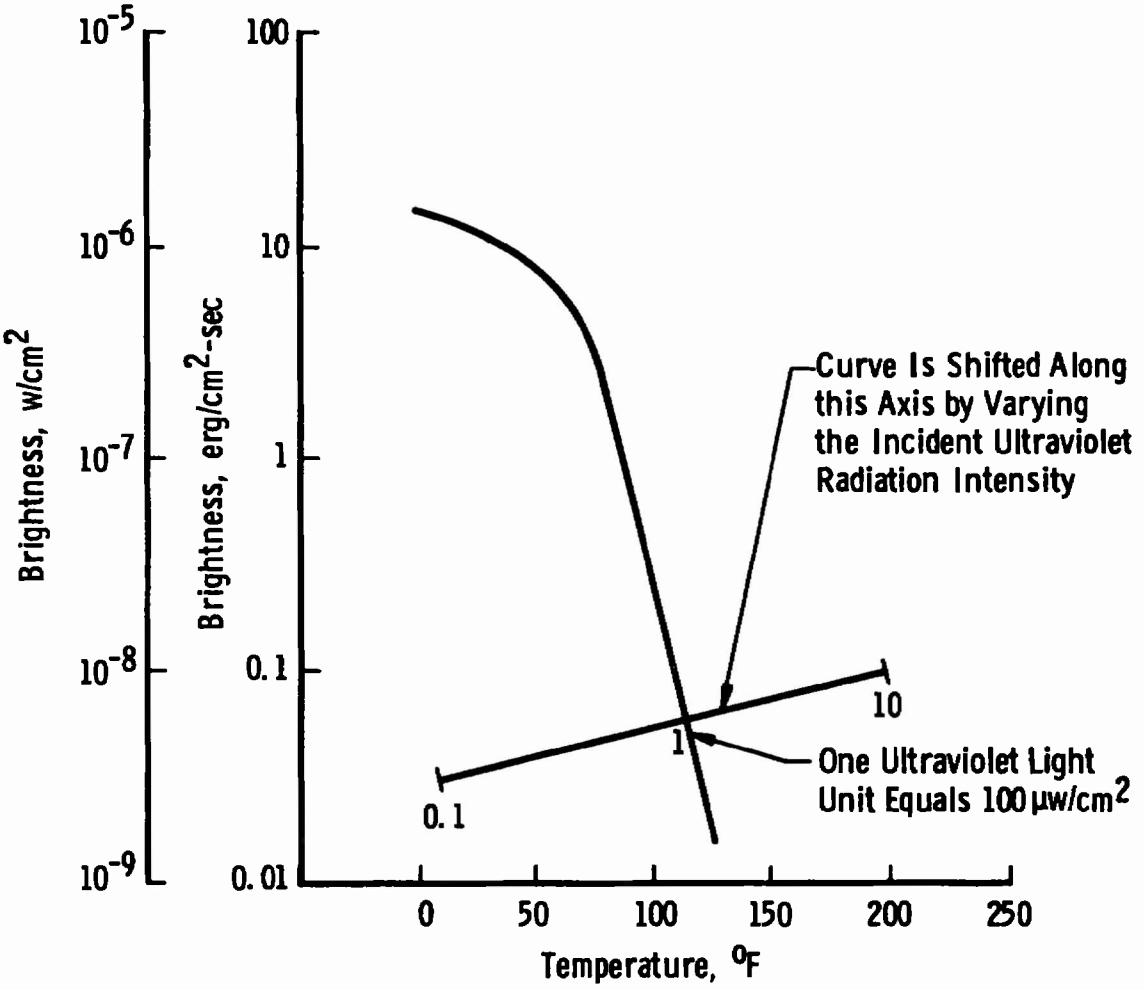

Fig. 5 Variation of Phosphor Brightness with Temperature for U. S. Radium Radelin® #1807 Phosphor

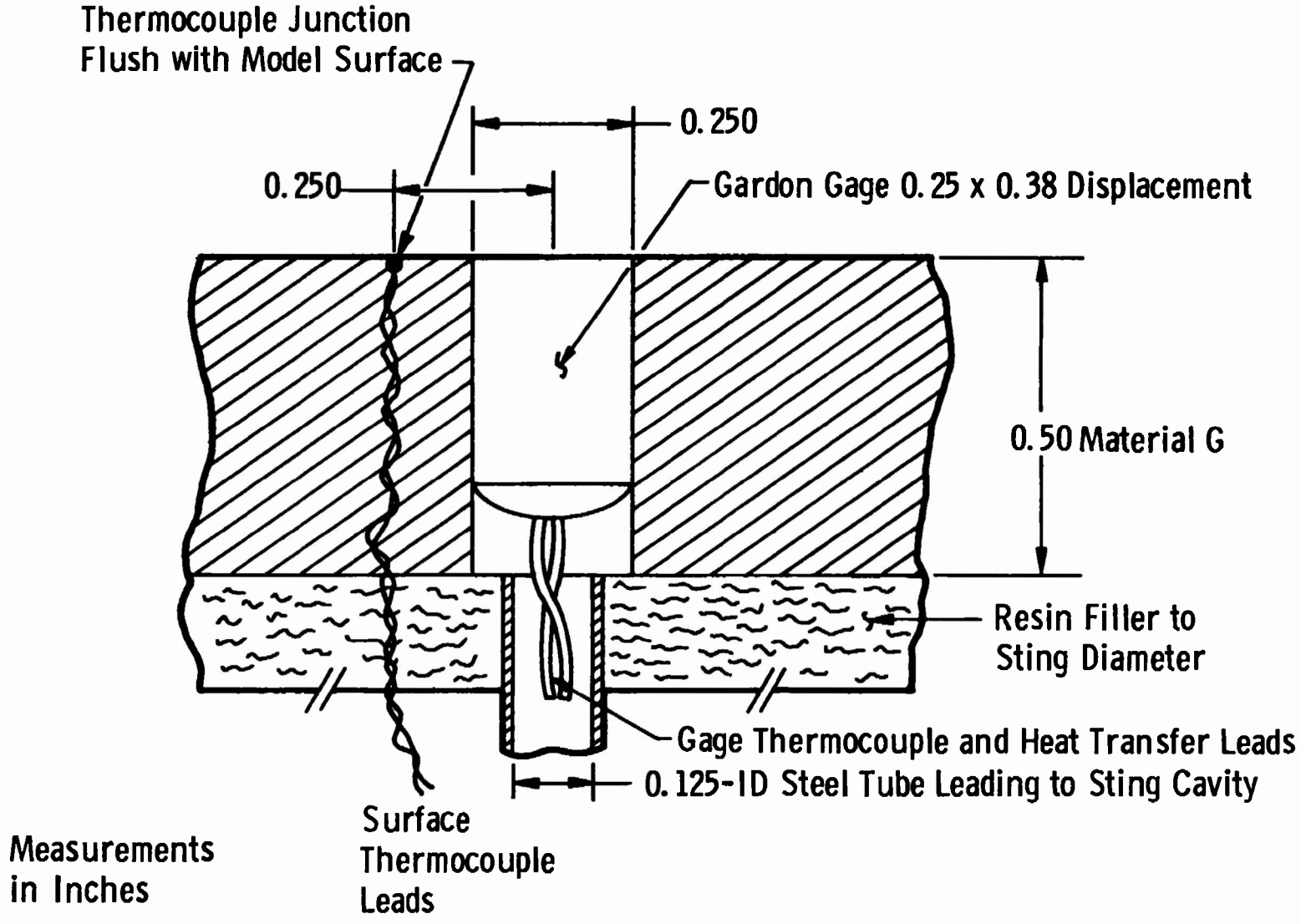

Fig. 6 Sketch of Gardon Gage and Surface Thermocouple Model Installation

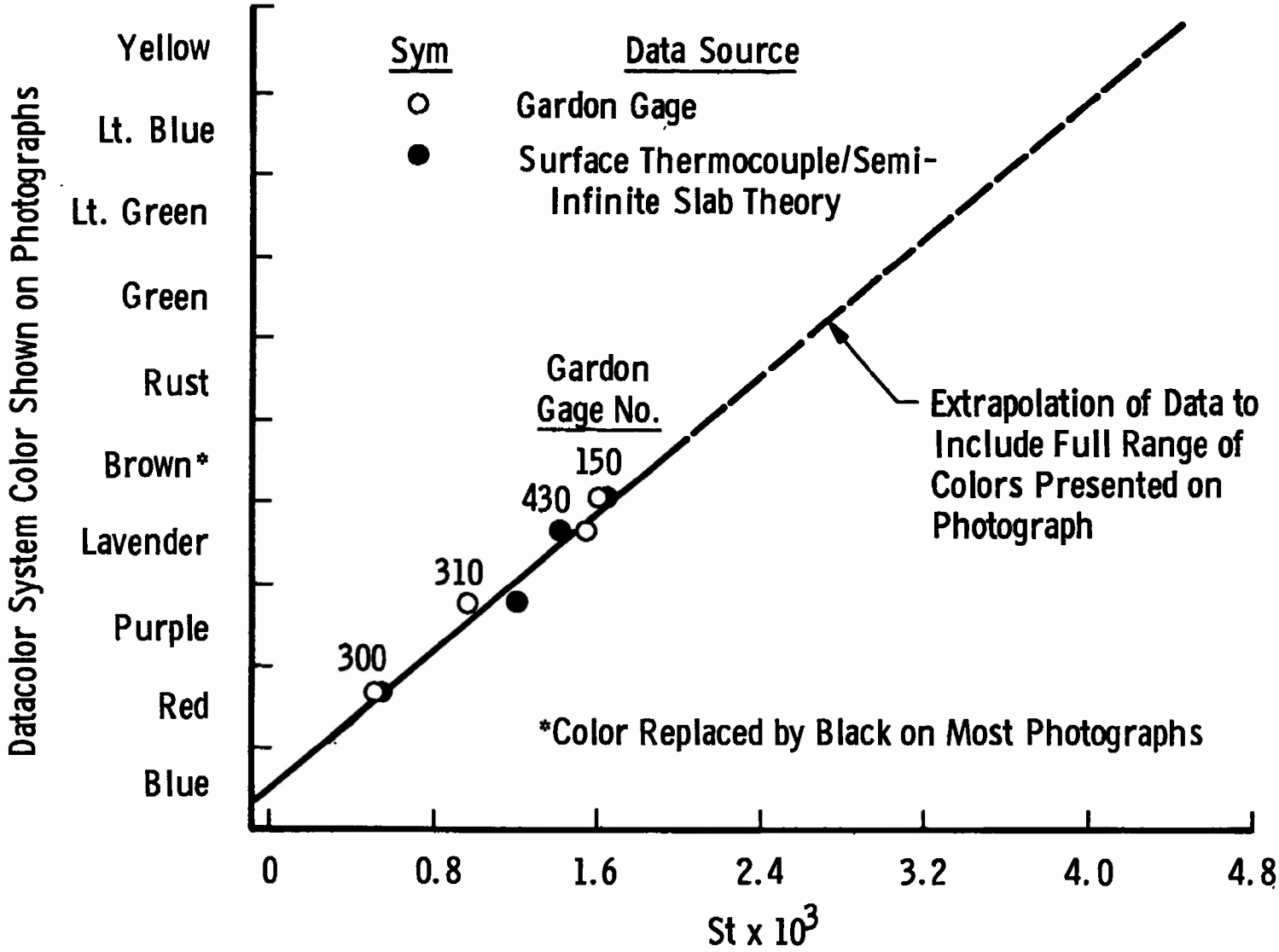

Fig. 7 Calibration Curve for Camera 1, 0.5-Scale Model, δ_c = 5 deg, α = 0, Showing How Data Color Is Related to Measured Stanton Number

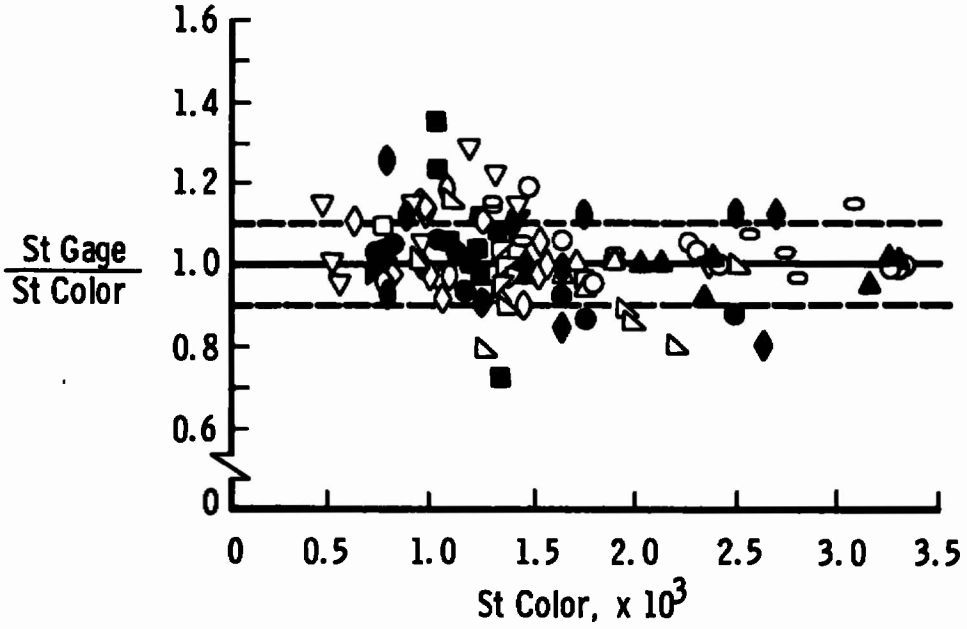

a. Stanton Number Ratio Distribution

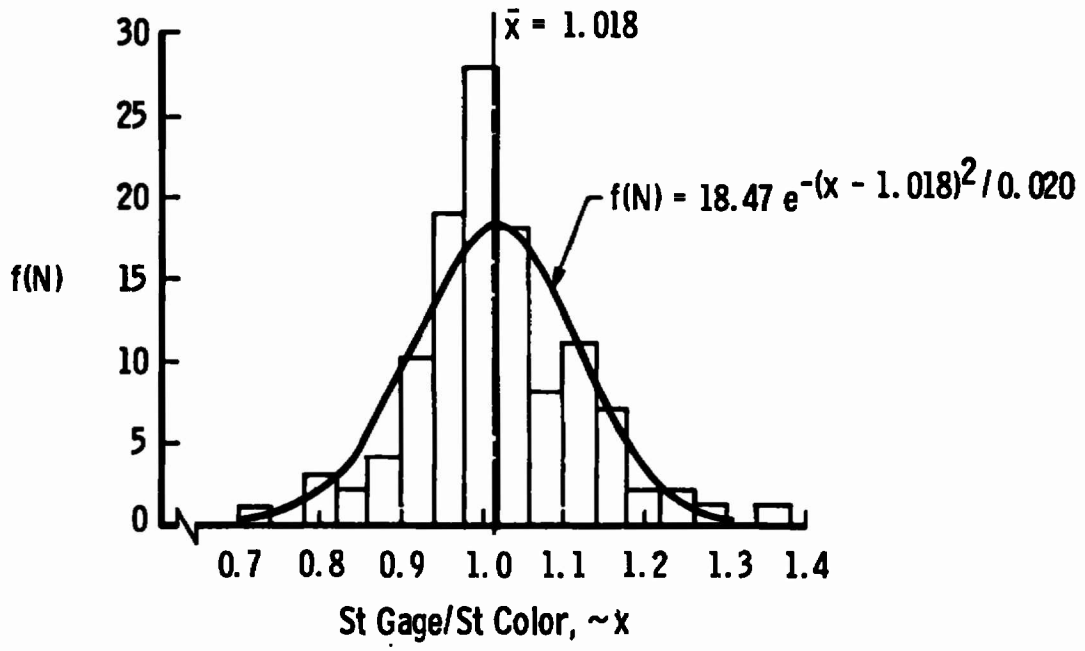

b. Normal Frequency Distribution

Fig. 8 Comparisons of Measured and Color-Indicated Stanton Numbers for Randomly Selected Data

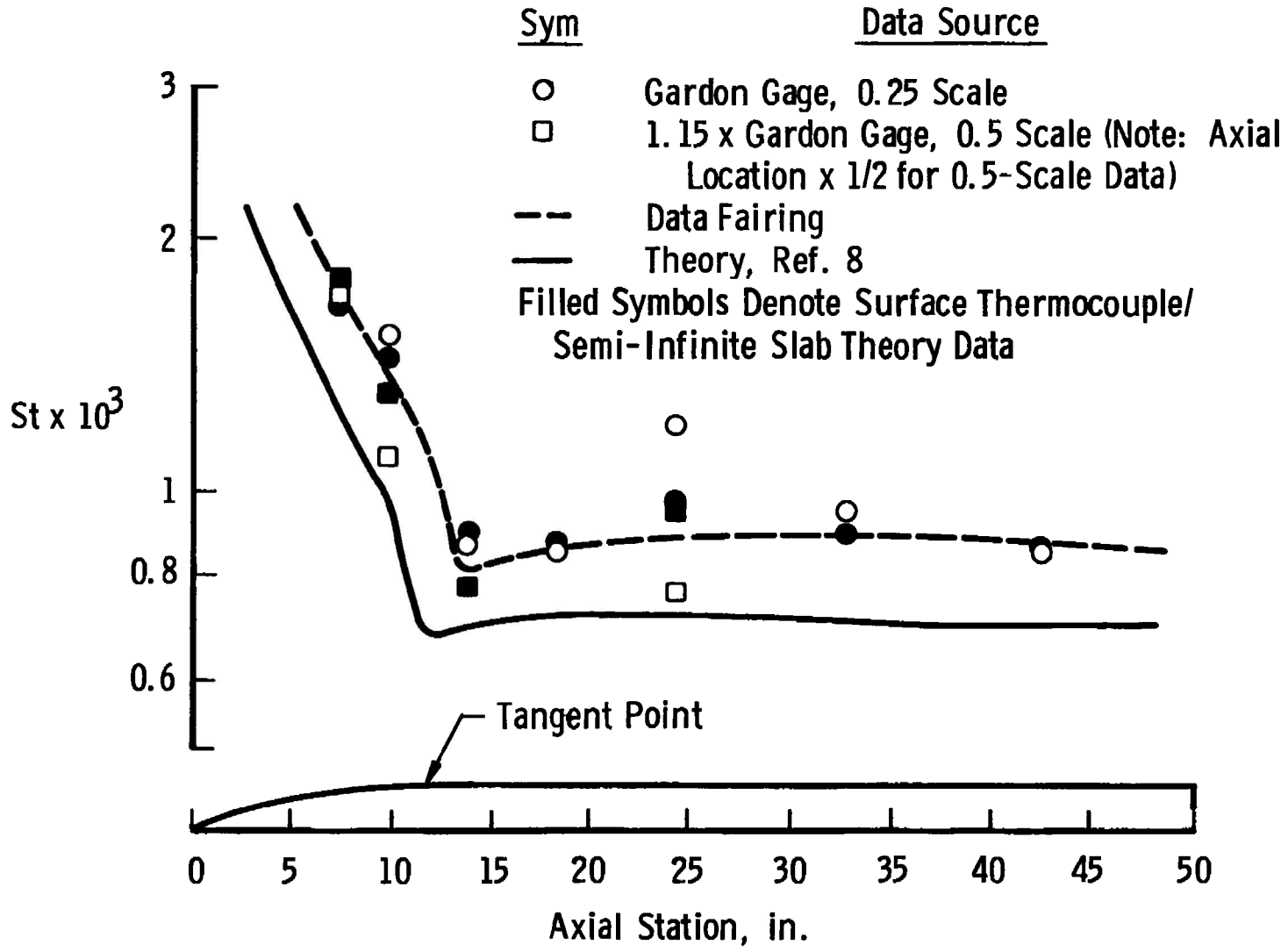

Fig. 9 Comparison of a Theoretical Calculation for Stanton Number Distribution with Measurements, δ_c = 15 deg, α = 0, $Re_\ell \approx 21 \times 10^6$, M_∞ = 4.03

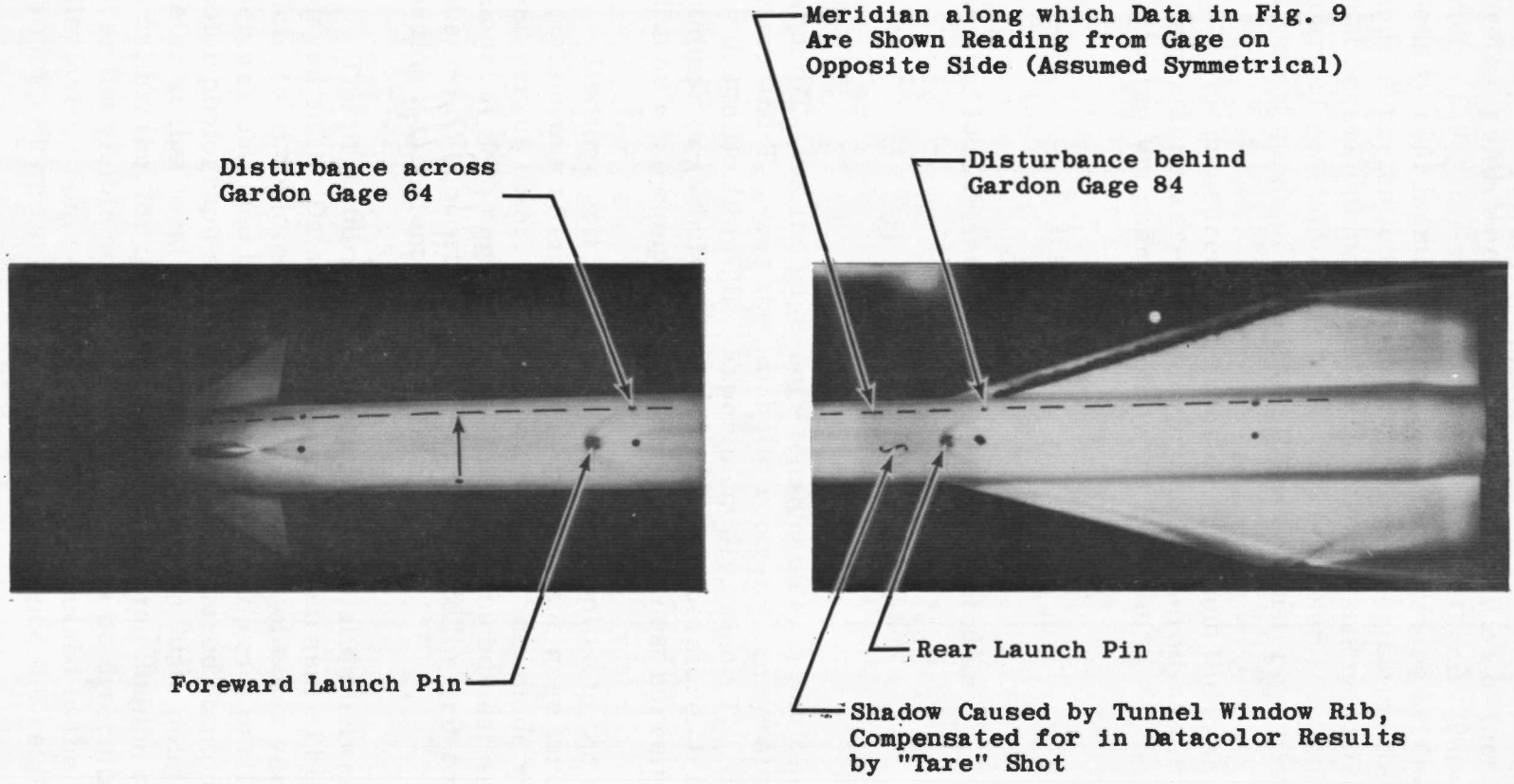

Fig. 10 Top View of 0.25-Scale Model Showing Heating Patterns, δ_c = 15 deg, α = 0, $Re_\ell \approx 21 \times 10^6$, $M_\infty = 4.03$

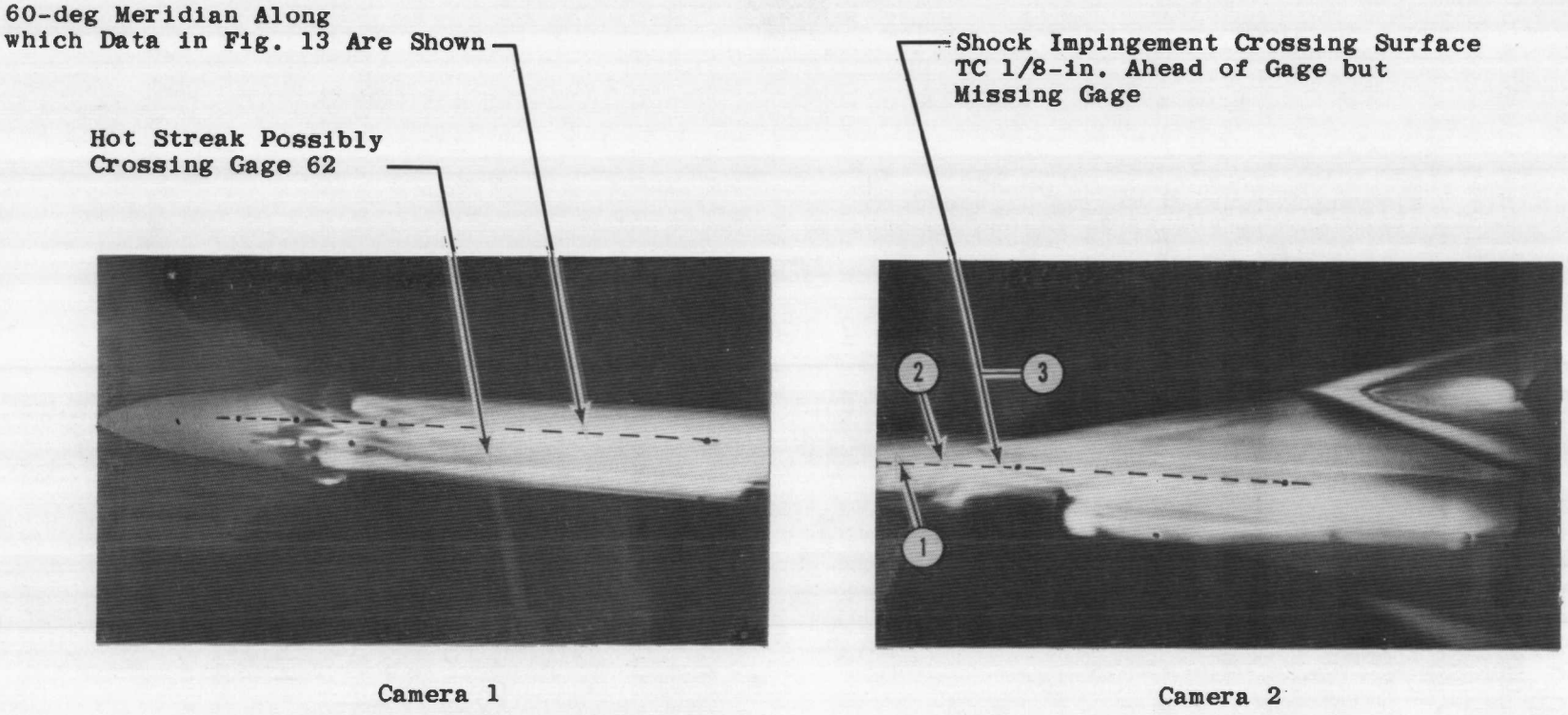

Fig. 11 Bottom-Side View of 0.25-Scale Model Showing Heating Patterns, δ_c = 15 deg, α = 4 deg, $Re_\ell \approx 21 \times 10^6$, M_∞ = 4.03

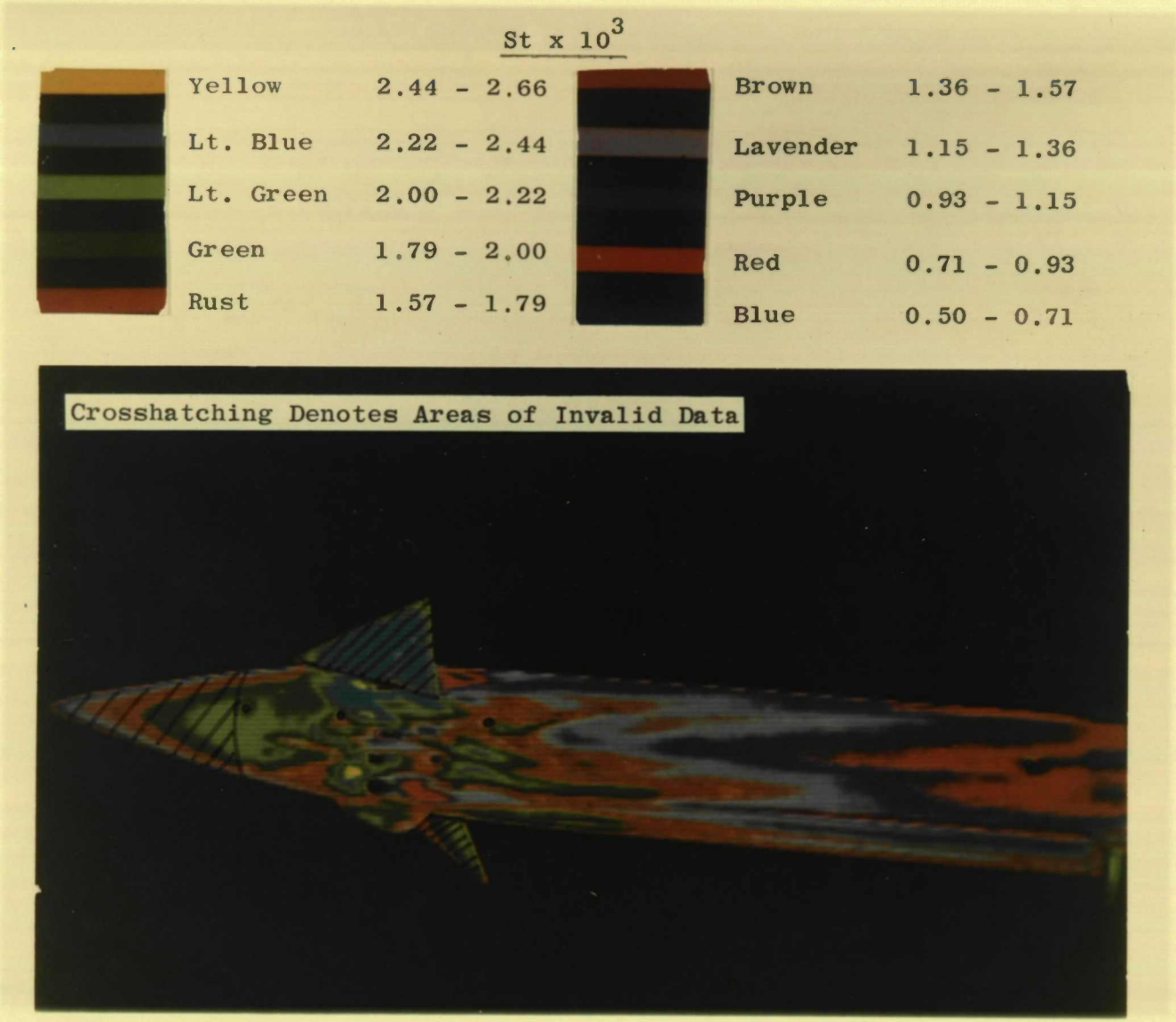

a. Camera 1—0.25-Scale Model, Front Half

Fig. 12 Photograph of Datacolor Analysis of Phosphor Brightness Variations Using Ten Color Increments, δ_c = 15 deg, α = 4 deg, $Re_\ell \approx 21 \times 10^6$, M_∞ = 4.03

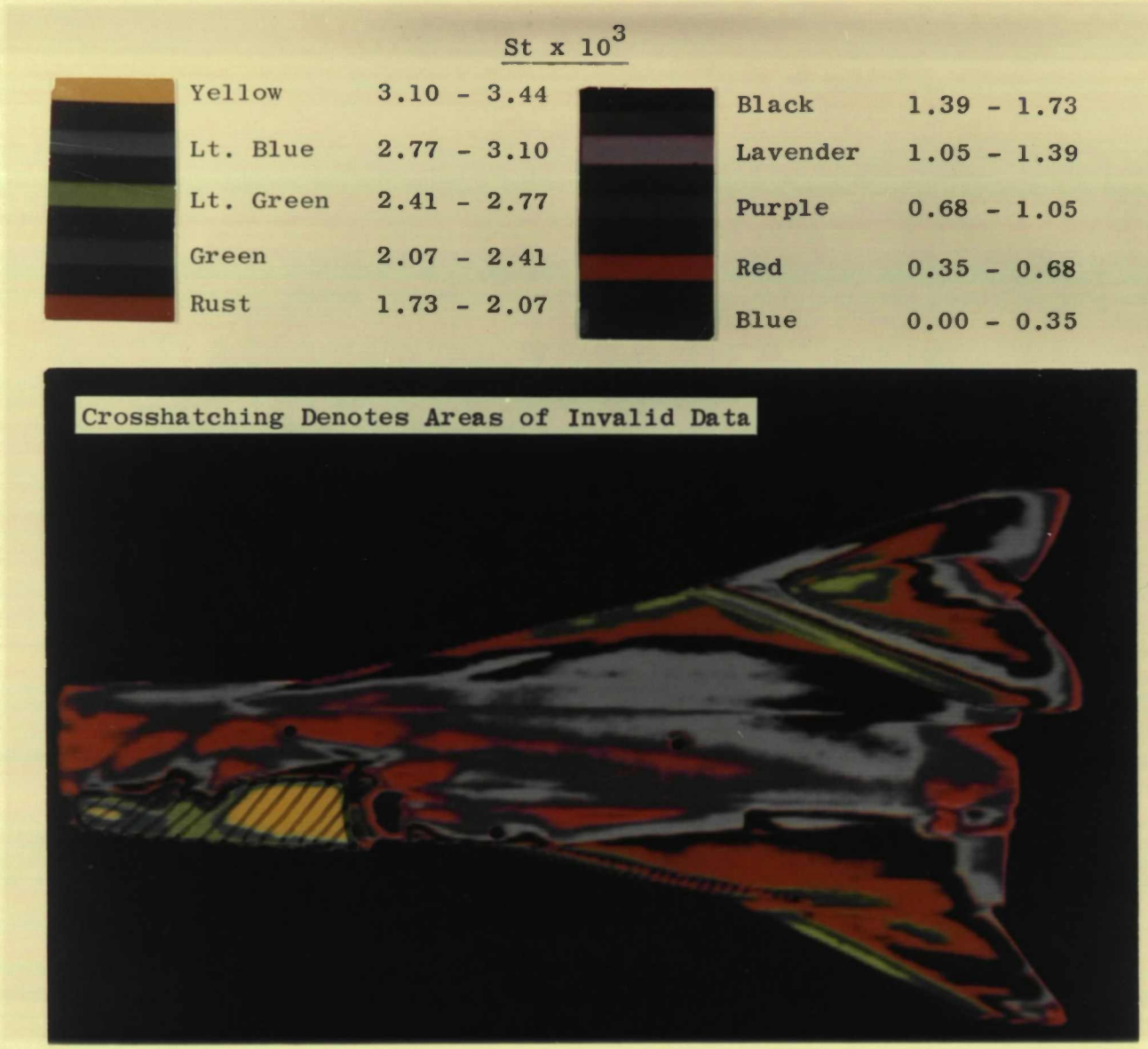

b. Camera 2—0.25-Scale Model, Rear Half
Fig. 12 Concluded

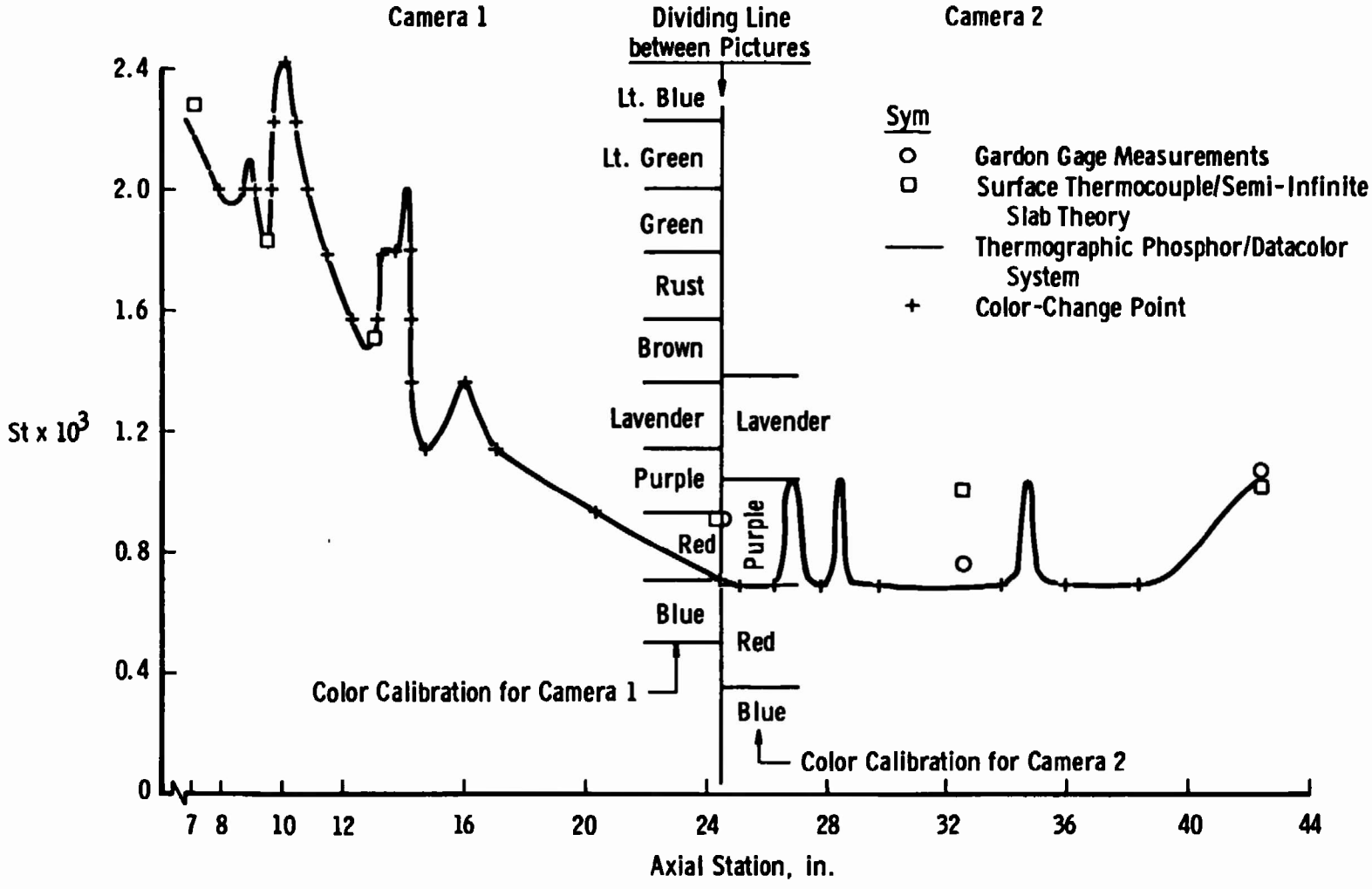

Fig. 13 Stanton Number Distribution Along a Line on Model Left Side 60 deg from Most Windward Streamline on 0.25-Scale Model, δ_c = 15 deg, α = 4 deg, $Re_\ell \approx 21 \times 10^6$, $M_\infty = 4.03$

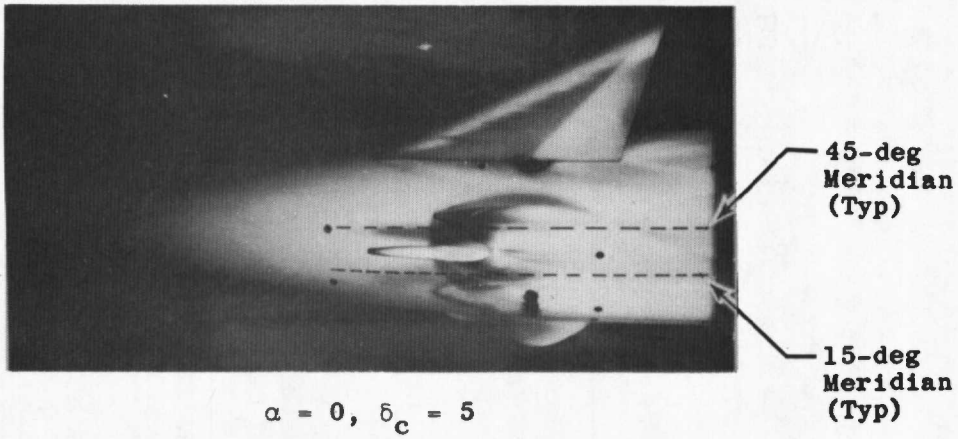

$\alpha = 0$, $\delta_c = 5$

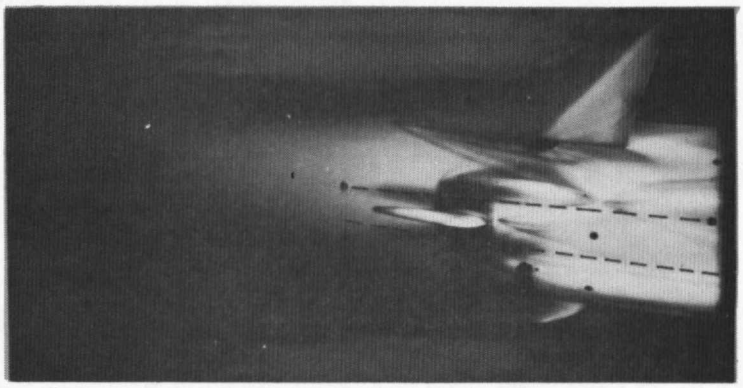

$\alpha = 8$, $\delta_c = 5$

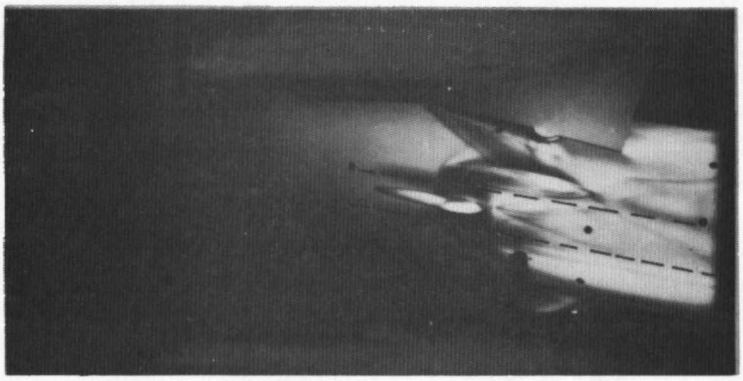

$\alpha = 12$, $\delta_c = 15$

Fig. 14 Photographs of the 0.5-Scale Model at Several Angles of Attack Showing the Regions of Most Intense Interference Heating, $Re_\ell \approx 21 \times 10^6$, $M_\infty = 4.03$

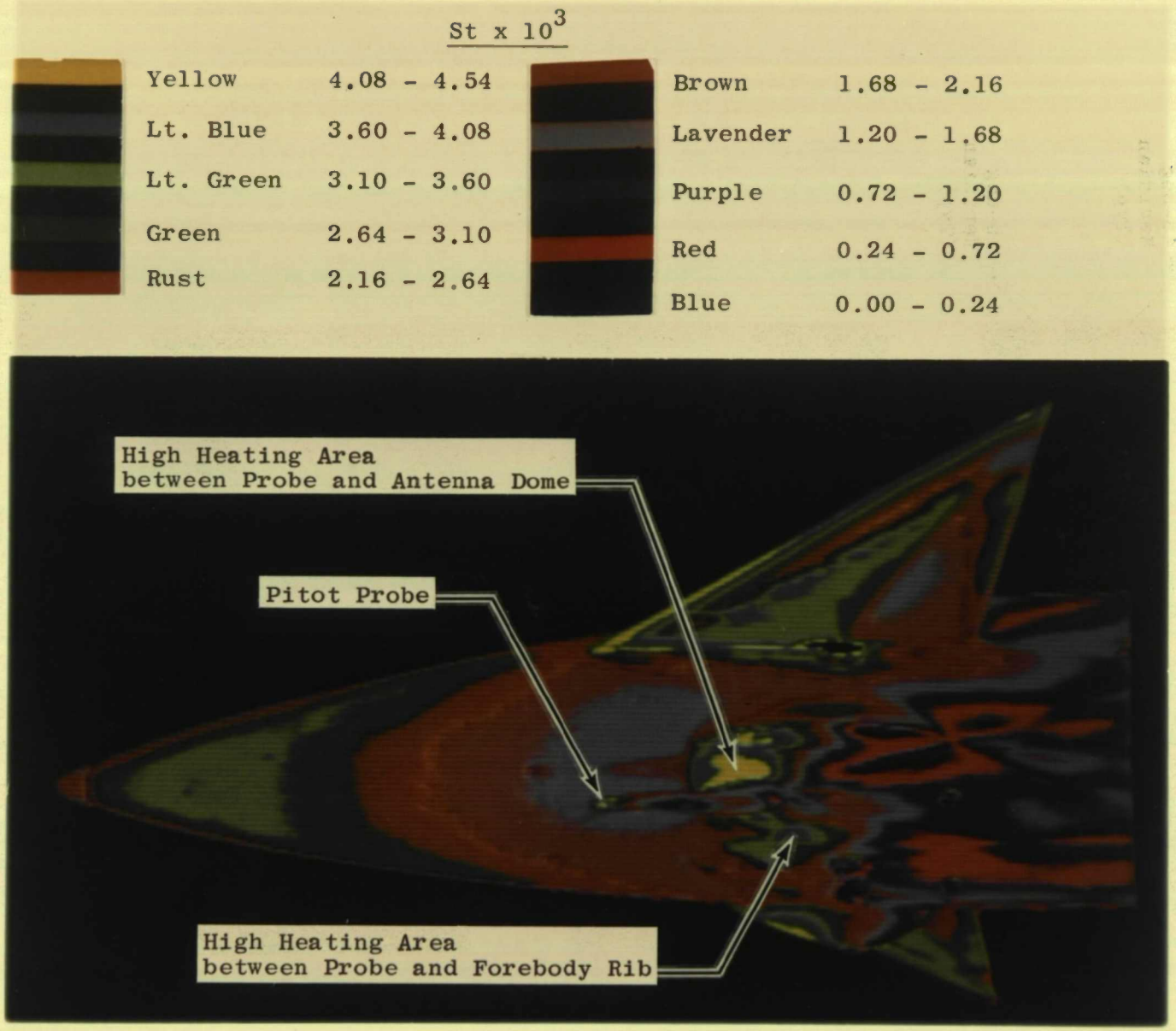

Fig. 15 Photograph of Datacolor Analysis of Phosphor Brightness Variations Using Ten Color Increments, δ_c = 5 deg, α = 0, $Re_\ell \approx 21 \times 10^6$, M_∞ = 4.03

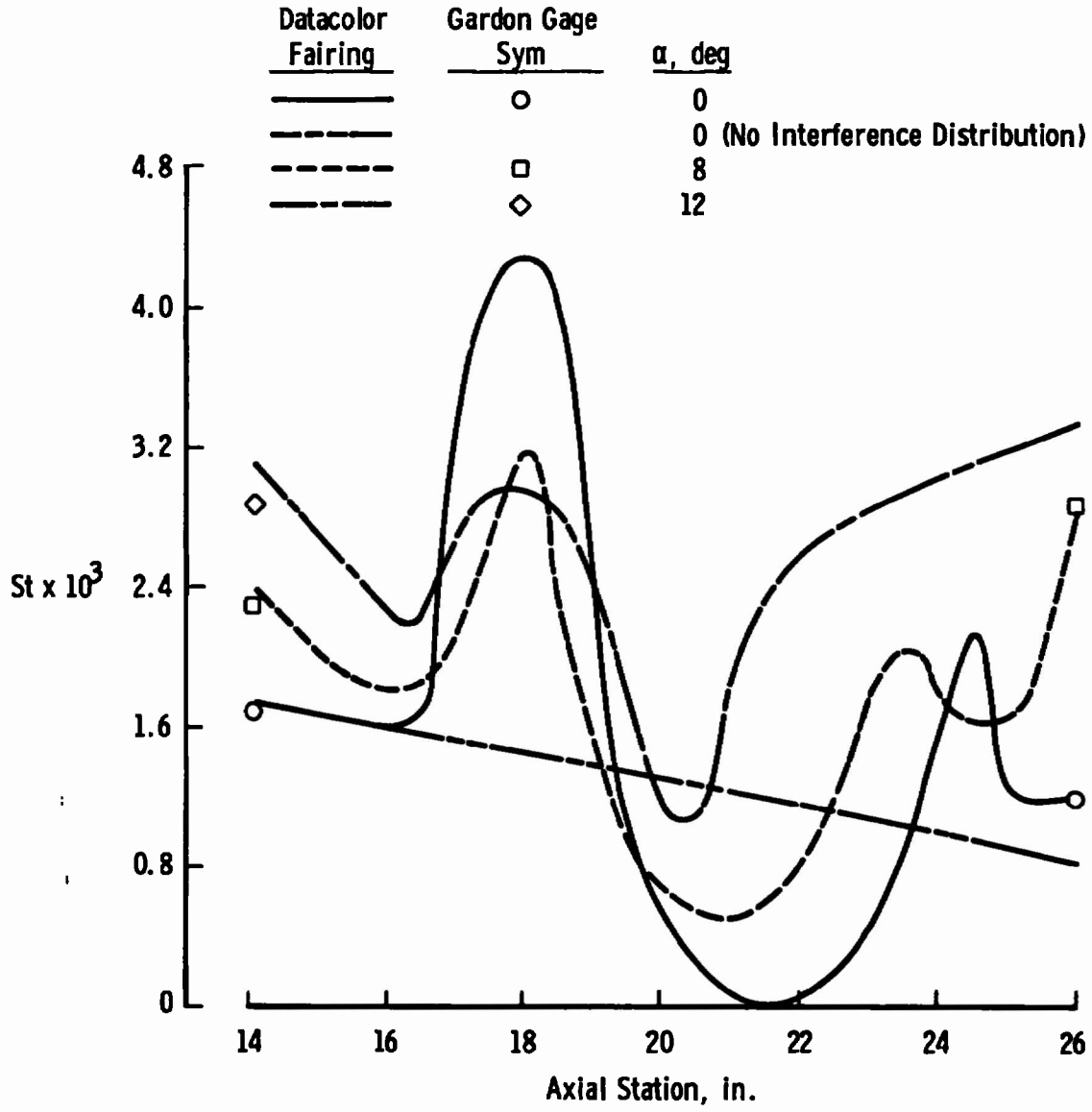

a. 45-deg Meridian

Fig. 16 Stanton Number Distributions Along Two Meridians of the 0.5-Scale Model Showing Variations in Heating Rate with Angle of Attack, $Re_{\ell} \approx 21 \times 10^6$, $M_{\infty} = 4.03$

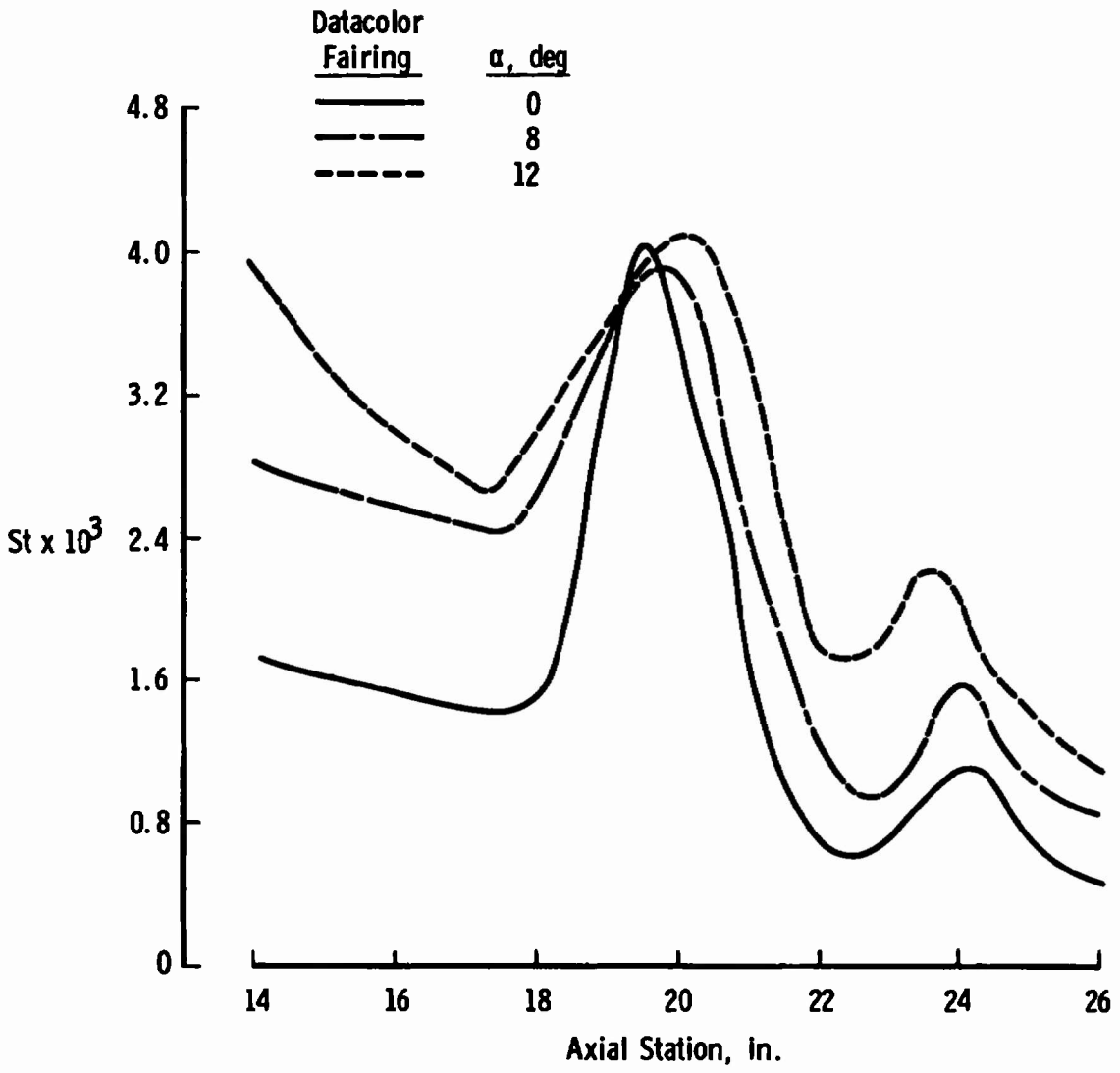

b. 15-deg Meridian
Fig. 16 Concluded

TABLE I
TEST SUMMARY

M_∞ = 4.03 p_o = 73 psia
$Re_\ell = 20.7 \times 10^6$ T_o = 660°R

Model Config.	Model Angle, α, deg	Canard Angle, δ_c, deg	Roll Angle, ϕ, deg	Canard Config.
0.5-Scale	0	2.33*, 5, 10, 15	0, 90	Mat'l. G
	0	5	45	
	4	5, 10, 15	0, 90	
	4	5	45	
	8	5	0, 45, 90	
	8	10	0	
	8	10, 15	0, 90	Metal
	12	15	0, 45	Metal
0.25-Scale	-8	0, 15	0, 90	Mat'l. G
	-4**	0, 15	0, 90	Mat'l. G
	0	0, 15	0, -90	Metal
	0***	0	-90	Metal
	4**	0, 15	0, 90	Mat'l. G
	4**	15	-135	Mat'l. G
	4**	15	0, -90	Metal
	8	0	0, -90	
	8	15	0, 90, -135	
	12	0, 15	0, -90	
	12	15	-135	

Grit roughness was applied on models as follows:

0.5 Scale: Carborundum® #54 1.5 in. from nose
*Carborundum #60 1.5 in. from nose

0.25 Scale: #40, 0.5 in. from nose and #46, 0.5 in. from upper and lower right wing leading edge

**#46 on nose and #54 on wing surface

***Nose trips removed

UNCLASSIFIED

Security Classification

DOCUMENT CONTROL DATA - R & D

(Security classification of title, body of abstract and indexing annotation must be entered when the overall report is classified)

1 ORIGINATING ACTIVITY (Corporate author) Arnold Engineering Development Center Arnold Air Force Station, Tennessee 37389	2a. REPORT SECURITY CLASSIFICATION UNCLASSIFIED 2b. GROUP N/A

3 REPORT TITLE

HEAT-TRANSFER TESTS USING THERMOGRAPHIC PHOSPHOR PAINT ON THE HIGH ALTITUDE SUPERSONIC TARGET (HAST) MISSILE AT MACH NUMBER 4

4 DESCRIPTIVE NOTES (Type of report and inclusive dates)

Final Report - February 21-22, 1972

5. AUTHOR(S) (First name, middle initial, last name)

E. C. Knox and L. D. Carter, ARO, Inc.

6 REPORT DATE February 1973	7a. TOTAL NO. OF PAGES 49	7b. NO OF REFS 8
8a. CONTRACT OR GRANT NO. b. PROJECT NO c. Program Element 63232F d. System 469A	9a. ORIGINATOR'S REPORT NUMBER(S) AEDC-TR-73-20 9b. OTHER REPORT NO(S) (Any other numbers that may be assigned this report) ARO-OMD-TR-72-139	

10 DISTRIBUTION STATEMENT Distribution limited to U.S. Government agencies only; this report contains information on test and evaluation of military hardware; January 1973; other requests for this document must be referred to Air Force Armament Laboratory (DLIV), Eglin AFB, FL 32542.

11 SUPPLEMENTARY NOTES Available in DDC	12. SPONSORING MILITARY ACTIVITY Air Force Armament Laboratory (DLIV) Eglin AFB, FL 32542

13. ABSTRACT

Thermographic phosphor heat-transfer tests were made on two models (0.5-scale and 0.25-scale) of the High Altitude Supersonic Target (HAST) missile at Mach number 4 and a Reynolds number, based on model length, of 21 x 10^6. Angle of attack was varied from 0 to 12 deg; effects of canard settings of 0 and 15 deg for the 0.25-scale model and 0, 5, 10, and 15 deg for the 0.5-scale model were examined. Comparisons of results by heat-transfer gages, thermographic phosphor, and surface thermocouple heat-transfer measurement techniques are presented. Color photographs showing heat-transfer-rate contours measured by the thermographic phosphor technique are included.

Distribution limited to U.S. Government agencies only; this report contains information on test and evaluation of military hardware; January 1973; other requests for this document must be referred to Air Force Armament Laboratory (DLIV), Eglin AFB, FL 32542.

DD FORM 1 NOV 68 1473

UNCLASSIFIED

Security Classification

14 KEY WORDS	LINK A		LINK B		LINK C	
	ROLE	WT	ROLE	WT	ROLE	WT
aerodynamic heating						
heat transfer						
temperature measurements						
supersonic flow						
thermocouples						